Proteomic analysis of S-nitrosylated nuclear proteins in rat cortical neurons

Authors: Smith J.G.[1], Aldous S.G.[1], Andreassi C.[1], Cuda G.[2], Gaspari M.[2], Riccio A.[1*]

Affiliations: [1]MRC Laboratory for Molecular Cell Biology, University College London, UK.

[2]Department of Experimental & Clinical Medicine, University of Catanzaro, Italy

*to whom correspondence should be addressed: a.riccio@ucl.ac.uk

One Sentence Summary: Proteomic analysis of rat cortical neurons revealed that over 600 nuclear proteins are modified by S-nitrosylation, including proteins involved in the regulation of gene expression such as CREB and RBBP7.

Abstract: The ability of neurons to modulate gene expression in response to extrinsic signals is necessary for proper brain function. S-nitrosylation is the covalent attachment of a nitric oxide (NO) moiety to cysteine thiols and is critical for transducing extracellular stimuli into specific patterns of gene expression. In the cerebral cortex, S-nitrosylation of histone deacetylase 2 (HDAC2) is required for gene transcription during neuronal development, however only few nuclear targets of S-nitrosylation have been identified to date. Here, we used S-nitrosothiol Resin Assisted Capture (SNORAC) coupled with mass spectrometry analysis to identify 614 S-nitrosylated nuclear proteins. Of these, 131 proteins had never been shown to be S-nitrosylated in any system, and 612 are new targets of S-nitrosylation in neurons. The site(s) of S-nitrosylation were identified for 59% of the targets, and motifs containing single lysines found at 33% of these sites. In addition, lysine motifs were found to be necessary for promoting S-nitrosylation of HDAC2 and Methyl-CpG Binding Protein 3 (MBD3). Moreover, S-nitrosylation of the histone binding protein RBBP7 was found to be necessary for dendritogenesis. Overall, our study provides the first extensive characterization of S-nitrosylated nuclear proteins in neurons and identifies putative S-nitrosylation motifs that may be shared with other targets of nitric oxide signaling.

Introduction

S-nitrosylation is a nitric oxide (NO)-dependent posttranslational modification that affects protein functions by regulating enzymatic activity, sub-cellular localisation or protein-protein interactions (*1-3*). Though over 3000 S-nitrosylated proteins have been identified to date, these include few nuclear proteins (*4-6*). In the rodent brain, expression of the enzyme responsible for neuronal nitric oxide production, the neuronal Nitric Oxide Synthase (nNOS) is developmentally regulated, and peaks during the mid-to-late embryonic stages during which the layered structure of the cortex is established (*7*). We previously showed that S-nitrosylation of histone deacetylase 2 (HDAC2) during this period results in dissociation of HDAC2 from chromatin, promoting histone acetylation and expression of CREB-dependent genes that are critical for neuronal migration (*4, 8*). S-nitrosylation of HDAC2 is also important in the adult brain; in the hippocampus for example, S-nitrosylation of HDAC2 is required for the updating of fear memories (*9*). Other examples of nuclear S-nitrosylation include glyceraldehyde 3-phosphate dehydrogenase (GAPDH), which is S-nitrosylated in the cytoplasm and translocates in the nucleus where it trans-nitrosylates several proteins, including HDAC2 (*5, 10*). Moreover, the transcription factor myocyte enhancer factor 2C (MEF2C) is S-nitrosylated in neurons in response to excitotoxic insults, resulting in reduced transcriptional activity and increased cell death (*6, 11*).

Previous proteomic screens provided few nuclear targets of S-nitrosylation in mammalian cells (*12-14*). To identify nuclear proteins that are potential targets of S-nitrosylation in neurons, we performed S-nitrosothiol Resin Assisted Capture (SNORAC) (*15*) on nuclear extracts of rat cortical neurons treated with CysNO. Mass spectrometry identified 614 nuclear targets of S-nitrosylation, as well as the site(s) of S-nitrosylation for most hits. In addition, Motif-X analysis revealed four lysine-containing motifs that promote S-nitrosylation of nearby cysteines. We found that proteins involved in metabolism, development and regulation of gene expression were modified by S-nitrosylation. Most subunits of the chromatin remodelling complex Nucleosome Remodelling and Deacetylase complex (NuRD) were found to be S-nitrosylated. Further analysis of the histone binding protein retinoblastoma binding protein 7 (RBBP7) revealed that S-nitrosylation at cysteine 166 was required for activity-induced dendritogenesis and regulated its interaction with the Chromodomain Helicase

DNA 4 (CHD4) subunit. The transcription factor CREB were also found to be S-nitrosylated in response to CysNO donors and following neuronal depolarisation. Our study provides the first SNO-proteome of neuronal proteins that may be used to study the function of nuclear S-nitrosylation in neurons in vitro or during cortical development in vivo.

Results

Identification of S-nitrosylated nuclear proteins in cortical neurons

To obtain a comprehensive analysis of nuclear S-nitrosylation in neurons, nuclear extracts from E17 rat cortical neurons were treated with the NO donor CysNO, and S-nitrosylated proteins were isolated using SNORAC (**Fig.1A**) (*15*). Eluted proteins were subjected to SDS-PAGE and silver staining to assess total SNO-proteins (**Fig.1B**). As a control, we used HDAC2 (**Fig.1B** and **Fig.S1A** and **Fig.S1B**), a known nuclear target of S-nitrosylation (*4, 5, 8, 9*). Corresponding samples were analysed using quantitative mass spectrometry (LC MS/MS, see **Methods**) to obtain the identification of SNO-proteins and the respective sites of S-nitrosylation. 71.75% of the identified proteins were detected as increased in CysNO-treated samples (**Fig.1C**), indicating that the SNORAC technique allows a significant enrichment of S-nitrosylated proteins. The remaining proteins were either unchanged across conditions (24.37%) or enriched in controls (3.88%), and were excluded from further analysis. 5 experiments were carried out in total; 2 using CysNO at a 1mM concentration and 3 using 200µM CysNO (**Table S1** and **Fig.S1C-E**). Despite variability in the number of SNO-proteins identified in each experiment (**Table S1** and **Fig.S1C**), 88.2% of the proteins identified using 1mM CysNO were also S-nitrosylated using 200µM CysNO (**Fig.S1D**), indicating that at both concentrations CysNO induced robust S-nitrosylation of a similar set of proteins. Proteins were designated as S-nitrosylated if they were enriched ≥2 fold in CysNO *versus* control samples in at least 3 independent experiments (See **Methods** for a description of the criteria used). 614 S-nitrosylated proteins (SNO-Ps) met these criteria (**Table S2**), of which 131 (38.1%) were novel targets of S-nitrosylation across all systems assayed to date, whereas 612 (99.7%) had not been previously identified as targets of S-nitrosylation in neurons. A higher number of hits was found when the S-

nitrosylated protein datasets were analysed using stringency conditions of ≥1.3 fold in CysNO *versus* control samples in at least 3 independent experiments (**Table S3**) or ≥1.5 fold in CysNO *versus* control samples in at least 2 independent experiments (**Table S4**). We also probed experiments 1-4 for proteins that are basally S-nitrosylated, by searching for proteins detected as unchanged in CysNO vs Cys, but increased in CysNO versus CysNO w/o ascorbate (**Table S5**). We observed that these proteins did not overlap with proteins detected as unchanged across all conditions (**Table S6**).

Gene ontology (GO) analysis of nuclear SNO-Ps

To determine whether certain types of proteins were enriched in our dataset, GO overrepresentation analysis (PANTHER GO analysis, see **Methods**) was carried out on the SNO-P dataset. First, untreated nuclear extracts from E17 cortical neurons were analysed by MS to generate a reference nuclear proteome of 3078 proteins (**Table S7**). Using this dataset as background, we found that 4 pathways were significantly enriched in the SNO-P dataset: Huntington disease (3.48 fold enriched), dopamine receptor mediated signalling (4.09 fold enriched), Wnt signalling (2.61 fold enriched) and nicotine pharmacodynamics pathway (5.41 fold enriched) (**Fig.S2A**). Annotations for molecular functions (**Fig.S2B**) indicated that chromatin-binding proteins were significantly enriched in the SNO-P dataset (1.99 fold). Whilst several terms associated with regulation of protein binding were overrepresented in SNO-Ps (**Fig.S2B**), hydrolase activity was the only term linked to regulation of protein activity (1.85 fold). Overrepresentation analysis for biological processes revealed that 4/29 terms assigned (13.8%) related to metabolic processes (**Fig.S2C**), whereas 4/29 (13.8%) concerned development. Remarkably, 2 terms were associated with regulation of gene expression (gene expression, 2.50 fold, and positive regulation of gene expression, 1.47 fold; **Fig.S2C**). Nucleic acid binding proteins were amongst the enriched terms in regard to protein class (3.11 fold, **Fig.S2D**). A summary of standard GO classifications, that does not take into account the relative occurrence of each term compared to the background nuclear protein dataset is displayed in **Fig.S3A**. Overall, our data indicate that S-nitrosylation of nuclear proteins may represent a mechanism that regulates metabolic, developmental and genetic processes.

In addition to nuclear extracts, corresponding extracts from the cytoplasmic compartment of E17 cortical neurons were exposed to CysNO and used to identify cytoplasmic SNO-Ps (see **Methods**, **Fig.S1B** and **Table S8**). As expected, our nuclear and cytoplasmic proteins datasets are largely distinct with 84.4% of detections unique to either dataset. GO analysis also revealed striking differences in annotations (**Fig.S3B-D**).

S-nitrosylation of nuclear factors in cortical neurons

We next sought to study S-nitrosylation of nuclear proteins that are involved in the regulation of gene expression and are especially relevant for neuronal functions. We considered SNO-Ps annotated with the GO terms transcription, DNA-dependent (GO:0006351) (**Table S9**) and chromatin organization (GO:0006325) (**Table S10**). The transcription factor cAMP-responsive element binding protein 1 (CREB1) (**Table S9**, hit number 6) regulates the transcription of genes essential for differentiation and survival of cortical neurons (*16, 17*). We previously demonstrated that NO regulates CREB-dependent gene expression (*17*) and that S-nitrosylation of histone deacetylase 2 (HDAC2) is necessary for CREB-activated transcription (*4, 8*). However, whether CREB is S-nitrosylated in neurons remained unknown. To investigate S-nitrosylation of specific nuclear proteins, we used the biotin switch assay (*18*). In this assay, S-nitrosylated cysteines are labelled with biotin and subsequently isolated using streptavidin capture. Biotin switch performed on cortical neurons exposed to CysNO confirmed that CREB is S-nitrosylated (**Fig.2A**). Strikingly, depolarisation of cortical neurons with KCl also induced S-nitrosylation of CREB (**Fig.2B**).

The retinoblastoma binding protein 7 (RBBP7) (**Table S10**, hit number 6) is a histone-binding protein associated with several chromatin-modifying complexes that regulate gene expression in neurons (*19-21*), including the NuRD complex. NuRD regulates cortical development in mouse (*19, 21*), however whether the subunits are post-translationally modified in response to extrinsic signals is unknown. We found that in cortical neurons, RBBP7 is S-nitrosylated in response to CysNO-treatment and depolarization (**Fig.2C** and **Fig.2D**) as well as following exposure to GSNO (**Fig.S4**). In addition to RBBP7, CHD3, CHD4 and CHD5, the ATPase subunits of the NuRD complex, were all detected as S-nitrosylated in the SNO-P dataset (**Table S2**, hit number 372, 373 and 87) and in

CysNO-treated HEK293T cell lysates (**Fig.S5**). Taken together, these findings demonstrate that our SNORAC screen identifies novel nuclear targets of S-nitrosylation, and suggest that S-nitrosylation may regulate chromatin remodeling complexes.

Identification of S-nitrosylated cysteines and putative S-nitrosylation motifs

To identify the cysteines modified by nitrosylation (SNO-sites), a second elution step was performed during SNORAC, which allowed the release of previously nitrosylated fragments from the resin. The fragments were then identified by LC MS/MS (**Fig.1A** and **Methods**). SNO-peptide analysis of experiment 5 detected 4368 cysteine-containing peptides in the CysNO sample (**Table S11**) and 1103 in the Cys control (**Table S12**). To identify SNO-sites, we analysed peptides detected in the CysNO dataset that belonged to proteins present in the SNO-protein dataset (**Table S2**). Using this approach, we assigned 942 unique SNO-sites across 360 proteins (**Table S13**). SNO-sites for proteins assigned using less stringent conditions are also provided (**Table S14** and **Table S15**).

Next, we searched for amino acid motifs that render certain cysteines more prone to nitrosylation, such as sequences containing acidic or basic residues either immediately flanking (*22*) or distal to the SNO-site (*23*). Motif-X (motif-x.med.harvard.edu, see **Methods**) revealed that lysine containing motifs were present in 277 of the 849 mappable SNO-sites (32.6%, **Fig.3A**). Whether specific lysine motifs are preferentially found in certain protein types in unknown, however GO analysis of proteins containing each lysine motif revealed differences in regards to annotations for biological process (**Fig.3B**). We investigated the functional relevance of the lysine(s) by assessing their effect on S-nitrosylation of the NuRD complex protein MBD3 (**Table S13**, hit number 271). SNO-site analysis was performed on MBD3 by generating DNA vectors expressing either the wild type protein or mutant forms bearing a mutation of the nitrosylated cysteines to serine (C215S and C266S), or mutation of lysine 264 to alanine (Lysine motif 1, K264A). CysNO-dependent S-nitrosylation of MBD3$^{C215S/C266S}$ was significantly reduced in HEK293T cells (**Fig.3C**), indicating that the cysteines identified by the SNORAC were indeed S-nitrosylated. Strikingly, K264 mutation either alongside C215S or alone also led to a drastic decrease of MBD3 S-nitrosylation. We previously demonstrated that HDAC2 is S-nitrosylated at C262 and C274 in neurons (*4*). Here, CysNO-induced S-nitrosylation

of HDAC2 was assessed upon mutation of HDAC2 lysine 280 to alanine (Lysine motif 2; K280A; **Table S13**, hit number 237) alone or in association with C262A (**Fig.3D**). Our findings indicate that a single lysine in the immediate area surrounding a cysteine is sufficient to promote S-nitrosylation at that site.

Sites of S-nitrosylation on CREB and RBBP7

To explore the physiological implications of S-nitrosylation of selected nuclear proteins, the site(s) of S-nitrosylation of CREB and RBBP7 were further investigated. SNO-peptide analysis failed to identify the cysteine(s) modified on CREB, possibly due to the small size of the predicted tryptic peptides (3, 5 and 6 amino acids) surrounding 3 of the 4 cysteines, which makes the peptides unsuitable for detection using mass spectrometry. Instead, CREB cysteine to serine mutant constructs were generated, and S-nitrosylation of the mutants was tested. CREB cysteines are located in the alpha domain (C90) and in the C-terminal bZIP domain that is important for CREB homodimerization and binding to DNA (C300, C310 and C337) (**Fig.4A**). Single mutants of C90, C300, C310 or C337 failed to reduce S-nitrosylation in CysNO-treated HEK293 cells, as did mutation of C300 and C310. However, triple mutation of C300, C310 and C337 led to a reduction in CREB S-nitrosylation (**Fig.4B**). CREB$^{C300/310/337S}$ was still phosphorylated at serine 133 in response to forskolin, suggesting that despite the mutations, the integrity of the protein and the ability to respond to intracellular signaling was preserved (**Fig.S6**).

SNO-peptide analysis identified C166 as the site of S-nitrosylation of RBBP7 (**Table S13**, hit number 238). C166 was previously identified as a potential site of S-nitrosylation on RBBP7 (*24*), however this finding had not been confirmed in intact cells. We generated a vector expressing a mutant form of RBBP7 carrying C166S mutation and found that S-nitrosylation of RBBP7 was abolished in CysNO-treated HEK293T cells (**Fig.4C** and **Fig.4D**). Since RBBP7 is closely related to RBBP4 (89.2% identical, 94.6% similar; **Fig.S7A**), we mutated the conserved cysteine in RBBP4 and found that this event also led to decrease S-nitrosylation (**Fig.S7B**). Because RBBPs function as scaffolding subunits for NuRD complexes, it is possible that S-nitrosylation provides a mechanism to regulate the assembly and stability of the complex.

7

NO regulates RBBP7 binding to CHD4

RBBP7 contains 7 WD (tryptophan-aspartic acid)-repeat regions, which provide platforms for protein binding and form a beta helical propeller structure (*25*). C166 of RBBP7 is within WD repeat 2 (**Fig.4C**), therefore we reasoned that S-nitrosylation may regulate the interaction of RBBP7 with other subunits within chromatin remodelling complexes. We first investigated whether S-nitrosylation of RBBP7 influences its interaction with other NuRD subunits by performing pull down experiments on cortical neurons. Strikingly, treatment with CysNO resulted in increased binding of RBBP7 to the ATPase subunit CHD4 (**Fig.5A**). To test whether the interaction depends on nitrosylation of RBBP7 at C166, FLAG-CHD4 was transfected with either HA-RBBP7^{WT} or HA-RBBP7^{C166S} in HEK293T cells, and the interaction was studied using pull down assay. We observed that CysNO increased CHD4 binding to RBBP7 (**Fig.5B**), and this effect depended on RBBP7 nitrosylation at C166. Thus, S-nitrosylation of this cysteine regulates the interaction between at least two subunits within the NuRD complex, perhaps determining its assembly on chromatin.

S-nitrosylation of RBBP7 promotes dendritogenesis in cortical neurons

In cortical neurons, NO signalling enhances dendritogenesis (*26*) by S-nitrosylating the RBBP7-interacting protein HDAC2 on C262 and C274 (*4*). We therefore investigated whether S-nitrosylation of RBBP7 may contribute to this process. Mouse embryonic cortical neurons were maintained under depolarising conditions with KCl (50 mM) for 2 days, and dendritic complexity was assayed using Sholl analysis. Knockdown of RBBP7 alone did not inhibit KCl-induced dendritogenesis (**Fig.S8A-B**), possibly due to the fact that the RBBP7 paralog RBBP4, S-nitrosylated at the conserved cysteine (**Fig.S7B**), and may be functionally compensating for RBBP7. Indeed, knockdown of both RBBP7 and RBBP4 led to a remarkable reduction of dendritic growth (**Fig.5C and Fig.S8C**). Strikingly, this effect was rescued by co-transfection of a rescue construct expressing RBBP7^{WT} but not RBBP7^{C166S}, indicating that S-nitrosylation of RBBP7 is required for dendritogenesis in vitro (**Fig.5C** and **Fig.S8D**).

Discussion

In this study, we identified the nuclear SNO-proteome of rat cortical neurons. To our knowledge, this is the first comprehensive screen of nuclear targets of S-nitrosylation performed in mammalian cells. Identification of nuclear proteins in previous studies (*12-14*) may have been limited by the low abundance of nuclear proteins relative to cytoplasmic, which renders nuclear targets of S-nitrosylation less amenable for detection. To circumvent this limitation, we assayed nuclear extracts of cortical neurons exposed to the NO-donor CysNO. This technical approach yielded 614 putative targets of S-nitrosylation that are suitable for further investigation. Known intracellular targets of S-nitrosylation in neurons were identified in our study, including GAPDH (*10*), HDAC2 (*4, 9*) and nucleophosmin (*27*). It should be noted however that our CysNO-responsive dataset may have missed some intracellular targets of S-nitrosylation, given that similar to other biotin switch- related methodologies, the SNORAC allows the identification of a subset of S-nitrosylated proteins (*28*).

Proteins involved in the regulation of gene expression and neuronal development were overrepresented in S-nitrosylated nuclear samples. We previously showed that S-nitrosylation of HDAC2 promotes the expression of genes necessary for neuronal radial migration during mouse embryonic development (*4, 8*). nNOS levels increase drastically when cortical layers are formed (*7, 8*), therefore additional nuclear proteins may be targeted by S-nitrosylation at these time points to regulate corticogenesis. As an initial step towards exploring this possibility, proteins involved in the regulation of gene expression were subject to further investigation. Both the transcription factor CREB and the histone binding protein RBBP7 were S-nitrosylated in cortical neurons following depolarisation. How S-nitrosylation affects CREB function is unknown, however mutation of the cysteines within bZIP domain (C300, C310 and C337) has been shown to affect binding of the coactivator CRTC2 (*29*). We found that S-nitrosylation of RBBP7 at cysteine 166 is required for activity-dependent dendritogenesis. The implications of this finding may be far-reaching, given that disruption of dendritogenesis at early developmental stages impacts on adult dendritic morphology and causes an aberrant response to fear conditioning (*30*). Our data also indicate that S-nitrosylation of RBBP7 may play a role in regulating subunit composition of the NuRD complex. S-nitrosylation of RBBP7 promotes its interaction with the NuRD ATPase subunit CHD4, an event that is especially

relevant during corticogenesis when NuRD complexes undergo a developmentally-regulated subunit switch (*21*). We previously showed that the mutual inclusion of CHD subunits within the NuRD complex determines the expression of specific sets of genes during mouse cortical development (*21*). Intriguingly, S-nitrosylation could represent a key regulatory mechanism shared by most NuRD subunits that may regulate their assembly on chromatin. How S-nitrosylation affects protein conformation of NuRD subunits is unknown, however recent reports suggest that S-nitrosylation may promote disulphide bond formation within and between proteins, thereby inducing structural changes which can outlast that of the initial S-nitrosylation event (*31, 32*). Thus it is possible that transient S-nitrosylation of the NuRD complex may induce disulphide bond formation that will have long-term effects on the complec subunit composition and, as a result, on gene expression .

GO analysis of S-nitrosylated nuclear proteins revealed that metabolic proteins are especially modified by S-nitrosylation. This finding is in agreement with a previous S-nitrosoproteome analysis of adult mouse brain that found several metabolic pathways targeted by S-nitrosylation (*13*). Although the role of S-nitrosylation on nuclear metabolism in mammalian cells is unknown, an effect has been shown in plants, where many nuclear proteins are S-nitrosylated in response to pathogen signalling in plants (*33*). Moreover, during plant stress responses, S-nitrosylation of the protein arginine N-methyltransferase 5 (PMRT5) promotes dimethylation of the spliceosome and pre-mRNA splicing of stress-response genes (*34*). The function of chromatin remodelling complexes, including NuRD, is affected by the availability of metabolically-generated cofactors (*35*). Thus, S-nitrosylation of proteins involved in both nuclear metabolism and gene expression may be functionally linked in neurons.

Here, we identified 4 lysine-containing motifs that may render cysteines more susceptible to S-nitrosylation. Previous work suggested that acidic and basic residues located in the vicinity of cysteines render nitrosylation more chemically favourable in these regions (*22, 23*). In macrophages, specific S-nitrosylation motifs have been shown to guide the interaction between donor and acceptor proteins required for trans-nitrosylation (*36*) yet similar trans-nitrosylation motifs have yet to be identified in neurons. Here, we found that our newly identified lysine motifs are essential for S-nitrosylation of both MBD3 and HDAC2. The lysine motif 2 (……C…..K) has previously been

identified in a screen on GSNO-treated heart homogenates (*24*), but was been functionally characterised. Indeed, the mechanisms through which lysine motifs regulate S-nitrosylation of MBD3 and HDAC2 are currently unknown, however a recent bioinformatic analysis suggested that cysteines in close proximity to ubiquitinated lysines are more likely to be modified by S-nitrosylation (*37*), hinting at a possible interplay between cysteine S-nitrosylation and post-translational modifications at neighbouring residues. Our screen provides targets of nuclear S-nitrosylation in cortical neurons, the site(s) of S-nitrosylation for most identified proteins and characterise for the first time, lysine- motifs that regulates cysteine S-nitrosylation. Further investigation of the S-nitrosylated proteins identified in our screen will be needed to reveal the full impact of NO signalling on nuclear functions in developing neurons.

Materials and Methods

Animal Procedures

All animal experiments were approved by the UCL Animal Welfare and Ethical Review Body and carried out in accordance to appropriate UK Home Office licenses. Timed pregnant Sprague Dawley rats and C57BL/6J WT mice were used to prepare embryonic cortical neurons.

Preparation of cortical neurons

E17 rat cortices were isolated in cold dissection buffer (1x HBSS, 2.5mM Hepes pH 7.4, 30 mM D-glucose, 1 mM $CaCl_2$, 1 mM $MgSO_4$, 4 mM $NaHCO_3$) and digested in digestion buffer (1 mM Hepes pH 7.4, 20 mM glucose, 82 mM Na_2SO_4, 30 mM K_2SO_4, 6mM $MgCl_2$, 0.25mM $CaCl_2$, 0.001% Phenol Red, 0.126mM NaOH) plus 200 units papain activated with cysteine-HCL and neutralised to pH 7. Cortices were washed, dissociated and plated in plating media (MEM with 10% FBS, 5% HS and 1 mM glutamine). Cells were plated on 10 cm Nunc plates coated with 20 μg/ml poly-D-lysine and 2 μg/ml laminin at 12.5 million per dish and kept at 37°C, 5% CO_2. After 1 day in culture, media was replaced with supplemented neurobasal (NB with 1x B27, 1 mM glutamine, 1x penicillin-streptomycin and 10 μM FdU). Prior to stimulation, cells were starved for 16h by replacing 2/3 of media with neurobasal without B27 (1 mM glutamine, 1x penicillin-streptomycin and 10 μM FdU). E15.5 mouse cortices were isolated and digested as for rat cortices. Cells were plated on coverslips in 24 well plates coated with 40 μg/ml poly-D-lysine and 2 μg/ml laminin at 0.35 million per well and kept at 37°C, 5% CO_2.

Cell culture and transfections

HEK293T cells (ATCC® CRL-11268™) and Neuro2a cells (ATCC® CCL-131™) were cultured according to standard conditions. Cells were transfected using Lipofectamine 2000 in OptiMEM according to manufacturer's guidelines.

Biotin Switch Technique

S-nitrosylation is light sensitive and light can also react with ascorbate to induce artifactual signals, therefore all procedures involving detection or stimulation of S-nitrosylation were carried out in minimal light conditions using brown eppendorf tubes and foil covered polypropylene falcon tubes. No glassware/metalware was used to avoid contaminating metal species that could interfere with the reaction (*38, 39*). CysNO was prepared as previously described (*40*). Cys only was prepared as for CysNO, using BPC-grade water (Sigma W3513) in place of $NaNO_2$. Buffers were prepared as in (*15*) with additional buffers used as specified.

For neuronal samples, 3 x 10cm plates of E17 cortical neurons per sample were treated as appropriate. For HEK experiments, a transfected 6cm plate of HEK293T cells was treated per condition. Cells

were washed twice with ice cold PBS and harvested in cold HEN lysis buffer (100 mM Hepes, 1 mM EDTA, 0.1 mM neocuproine, pH 8.0 with 0.2% NP40). Samples were then homogenized 5 times with a 25-gauge needle, centrifuged for 10 min 10,000g 4°C and supernatant collected (neuronal samples contained ~1.2 mg of protein per 3 plates, HEK293T cells 650 µg of protein per sample). Except for experiments in Fig 2 that were lysed and blocked immediately, low molecular weight S-nitrosothiols were removed by acetone precipitation -20°C for >1h, followed by centrifugation of protein pellets for 20 min 2,000g 4°C, 2 washes with 70% acetone, and resuspension in 200µL HENS (100 mM Hepes, 1 mM EDTA, 0.1 mM neocuproine, pH 8.0 with 1% SDS). Samples ere blocked by adding an equal volume of 2X MMTS Blocking Buffer (2% MMTS, 5% SDS in HEN buffer) and incubated for 30 min at 50 °C with intermittent vortexing. Protein pellets were precipitated and as before, then washed 3 times with 70% acetone and resuspended in 220 µL HEN lysis buffer. Sodium ascorbate was added to a final concentration of 50mM and samples incubated for 5 min at RT with gentle mixing. Biotin HPDP (Thermo 21341) was added to 1 mM and samples rotated for 45 min, followed by acetone precipitation as above. Following 3 washes with 70% acetone, samples were resuspended in 220 µL HENS and 400 µL neutralization buffer added. Samples were precleared by incubation with protein A beads for 1h at RT, then centrifuged 500 g 5 min RT and supernatant removed. 10% total inputs were taken, and samples incubated with 30µL bead volume of streptavidin agarose beads overnight rotating at 4°C. Samples were then centrifuged for 500g 5 min 4°C, and washed 4 x in wash buffer (neutralization buffer 600 mM NaCl). Beads were dried using a 29G needle and 40µL of 2x western loading buffer (2% SDS, 2% βME, 20% glycerol, 100 mM Tris 6.8, 0.008% bromophenal blue) was added. Samples were then boiled for 5 min, then centrifuged 10,000g 2 min RT and supernatant run on homemade 10% polyacrylamide gels or precast NuPage 4-12% Bis-Tris gels (NP0335). For biotin switch on treated cellular lysates, the above protocol was followed, except treatment took place post harvesting in samples made up to 500µL with HEN buffer. In experiments using NEM blocking (140 mM in HEN buffer with SDS at 2.44%), blocking was carried out for 45 min at 50 °C.

SNORAC

Nuclear and cytoplasmic protein extractions of E17 neurons were carried out using the NE-PER kit (Thermo, cat no: 78833) as per the manufacturer's instructions, with an extra wash with CER1 prior to addition of buffer NER. 400 µg of protein was used per sample. CysNO treatment for 20 min was carried out in the CER1 (cytoplasmic) or NER1 (nuclear) buffer with intermittent mixing. CysNO was removed after treatment either by acetone precipitation or using P6 spin columns prewashed in HEN buffer. Protein amounts were equalized by BCA assay then volume made up to 500µL with HEN buffer. SNORAC was carried out according to (*15*) with the following modifications. Thiopropyl sepharose 6B resin (GE Healthcare, 17-0420-01) was used, after 3 washes in BPC water and 1wash in HEN buffer. Beads were centrifuged at 500 g 10 min 4°C in between washes. Beads were stored (no

longer than 1 day) at in HEN buffer at 4°C in a 1:1 ratio. Mass spectrometry samples were frozen with HEN buffer diluted 10 fold in water and stored at -20°C.

Silver staining

Standard silver staining protocol was followed. Briefly, the polyacrylamide gel was soaked in 50% methanol 2 x 15 min then 5% methanol for 10 min before rinsing in water. Gel was then soaked in 10 μM DTT for 20 min and then in 0.1% silver nitrate for 20 min. After 3 washes with water, gel was washed 2x in developer solution (500 mL ~285 mM sodium carbonate solution plus 250 μL 37% formaldehyde) and soaked until bands became visible. The reaction was stopped with addition of citric acid and gel washed in water before imaging.

Co-IP protocol

Co-immunoprecipitation experiments were performed in low light conditions (see sample guidelines for working with S-nitrosylation (*39*)). *For neurons*: 1x 10cm plate used per condition. Cells were treated with 200 μM CysNO donor or Cys control for 20 min and then washed with cold PBS and harvested in cold IP Lysis buffer (50mM Tris pH 7.4, 150mM NaCl, 1% TX100, 1% Sodium Deoxycholate) containing a protease inhibitor cocktail, phosphatase inhibitors 2 and 3 and PMSF (all at 1:100). Samples were lysed on ice for 30 min and homogenized and then cleared by centrifugation at 1000xg for 10 minutes at 4°C. Lysates were pre-cleared with protein G-Sepharose beads (GE healthcare, 17-0618-01) for 2 hrs at 4°C. Total inputs were taken. The remaining sample was incubated overnight 4°C with rabbit anti-CHD4 (ab72418) or rabbit IgG (Dako X0903). Lysates were then incubated with protein G–Sepharose beads for 2 hours at 4°C. Beads were washed 1x time with wash buffer (50 mM Tris pH 7.5, 150 mM NaCl, 0.1% TX100, 5% glycerol, protease and phosphatase inhibitors at 1:1000), 2x with wash buffer and 2 x PBS. Excess PBS was removed and proteins eluted by boiling the beads with 2x Western loading buffer. Total Inputs and samples were then run on precast 3-8% Tris-Acetate gels. *For HEK293T*: 6 cm plates of HEK293T cells were cotransfected with Flag mCHD4 and either HA-RBBP7$_{WT}$ or HA-RBBP7$_{C166S}$. HEK 293T cells were treated as for E17 neurons then washed with cold PBS and harvested in cold RIPA buffer (50 mM Tris pH 7.5, 150 mM NaCl, 1% NP40, 0.5% Deoxycholate) containing inhibitors as above at 1:100. Samples were lysed and cleared then protein concentration was determined using BCA Protein Assay; 250-400 μg of protein was used per experiment. Lysates were pre-cleared and total inputs were taken. Remaining sample was incubated overnight in the dark 4°C with rabbit anti-HA (CST 3724S) or rabbit IgG (Dako X 0903). Lysates were then incubated with protein G–Sepharose beads for 2 hours at 4°C. Beads were washed and proteins eluted as for E17 samples. Samples were then run on precast NuPage 4-12% Bis-Tris gels.

Western blotting

Western blot was carried out according to standard procedures. Transfer conditions were 100V for 3hrs at 4°C in 10% methanol for experiments involving detection of high MW proteins and were 330mA for 1 hr 30 in 20% methanol for routine transfers. Membranes were blocked in 5% Milk/TBST prior to overnight incubation at 4°C with primary antibodies at a 1:1000 dilution. The following primary antibodies were used: mouse anti-C-Myc (A7 Santa Cruz Sc-56634), mouse anti-Flag (M2 Sigma F3165), mouse anti-HA (Biolegend 901502), rabbit anti-HA (Cell Signaling, 3724), mouse anti-HDAC2 (Merck Millipore 05-814), mouse anti-HSP90 (Abcam Ab13492), rabbit anti-RBBP4 (Abcam 79416), rabbit-RBBP7 (Sigma R4279), goat anti-HSP90 (Santa Cruz Sc-1055), rabbit anti-CREB (CST 9197), phospho-CREB ser133 (CST 9191S). Post TBST washes, membranes were incubated with the appropriate secondary antibody at a 1:20000 dilution. Secondary antibodies: anti-mouse HRP GE Healthcare NXA931, ant- goat HRP Sigma A5420, anti-rabbit HRP GE Healthcare NA93AV. Signal was detected using ECL or ECL Prime detecting reagents (GE Healthcare Life Sciences) and by exposing the immunoblot to the Amersham Hyperfilm (GE Healthcare Life Sciences).

Dendritogenesis assay

E15.5 mouse neurons were transfected using Lipofectamine 2000 2 hr post plating, with 220 ng Pbird GFP with 500 ng of either mycEV, mycRBBP7$_{WT}$ siRNA resistant or mycRBBP7$_{C166S}$ siRNA resistant plasmids. Cells were co-transfected with 400nM of each siRNA. Media was changed 3 hr post transfection to Neurobasal media supplemented with 0.33% B27, 1 mM glutamine, 1x penicillin-streptomycin and 10 μM FdU, and coverslips fixed in 4% PFA/PBS 48 h post transfection. Coverslips were washed 1x PBS, permeablised in 0.3% Triton-X/PBS and blocked in 5% NGS 5% FBS/ PBS for 1 hr RT, and incubated with chicken anti-GFP (Abcam ab13970) overnight. After 3 PBS washes, samples were incubated with Dapi and Alexa Fluor goat anti-chicken 488 (Life Technologies A-11039) at 1:1000 for 1hr RT. Coverslips were washed and mounted. Slides were then blinded prior to imaging and analysis. Images were acquired using SPE or SPE3 confocal microscope (Leica) with LAS AF software and processed using ImageJ/Fiji. Sholl analysis was performed using Image J Simple Neurite Tracer (Fig.S8) or Fiji sholl analysis plugin (Fig.4), and samples de-blinded after final processing.

Plasmids

The CMV myc-CREB plasmid was created by Bonnie Lonze (Ginty Lab). msMBD3, ratRBBP4 and ratRBBP7 were subcloned into the CMV-myc expression vector. Mutagenesis to create RBBP7, RBBP4 and MBD3 cystine-to-serine mutants, MBD3 lysine-to-alanine, and mycRBBP7$_{WT}$ and mycRBBP7$_{C166S}$ siRNA resistant plasmids was carried out using Quikchange multisite-directed

mutagenesis kit (Agilent). HA-tagged ratRBBP7 and HA-tagged msHDAC2 were each cloned into Adeasy pshuttle CMV vectors, and cysteine and lysine mutants created using Quikchange multisite-directed mutagenesis kit (Agilent). Flag mCHD4, hCHD5 and hCHD3 were generated as previously described (*21*). SiRNAs were generated by Invitrogen. Sequences: siRBBP7 (5'-3) CCA CAU AAU GAA ACU AUU CUG GCU U and the reverse complement (5'-3') AAG CCA GAA UAG UUU CAU UAU GUG G. siRBBP4: (5'-3') AAA UCU UUC CCU UCA GGC CUG GUC A and the reverse complement (5'-3') UGA CCA GGC CUG AAG GGA AAG AUU U.

Statistical Analysis

Statistical analysis was performed as indicated in figure legends. All analysis was performed using GraphPad Prism Software (Version 7.0a).

Gene Ontology Analysis

Neuronal screens: Classifications listed on tables assigned from Uniprot by Proteome Discoverer 1.4 (Thermo Fisher Scientific, Bremen, Germany). All other gene ontology analysis was carried out using PANTHERdb (pantherdb.org) and version number listed in the respective figure legend.

Overrepresentation Analysis: PANTHER Overrepresentation Test (release 20170413) with Bonferroni correction for multiple testing. For Figure S2. nuclear protein background dataset (Table S7) was used as background dataset.

Mass Spectrometry

CysNO-treated neuronal extracts (1mM CysNO)

Exp. 1
A1. 1 mM Cys
A4. 1 mM CysNO
A5. 1 mM CysNO without ascorbate
Exp. 2
B1. 1 mM Cys
B2. 1 mM CysNO
B4. 1 mM CysNO without ascorbate

Beads thawed at 4 °C, centrifuged 4000 rpm 1min RT. Supernatant was digested at 37 °C with 800 ng of trypsin proteomics grade (Sigma) in 100 µL of 100 mM tris buffer, pH 8.5 (buffer A). Following

tryptic digestion, supernatants were recovered. Beads were washed three times with 20 mM ammonium bicarbonate in 50% MeOH (v/v) (buffer B). Ammonium bicarbonate washes were pooled, dried, then combined with the first supernatant.

Quantitative analysis: Digested proteins samples were subjected to O^{18} labelling as in (*41*). 30 µL aliquots of **A**-4, **A**-5, **B**-1, **B**-2 were dried and resuspended in 50 µL of H_2O^{18} 98% pure (Sigma) / methanol 4:1 (v/v). Solution was then buffered by the tris buffer. A fresh trypsin aliquot (200 ng in 0.5 µL) was added in order to catalyse the oxygen exchange reaction, which was allowed to proceed overnight at 37 °C. 30 µL aliquots of **A**-1, **A**-4, **B**-2, **B**-4 were dried, resuspended in 30 µL of normal HPLC water, and subjected to a parallel trypsin-catalysed oxygen exchange reaction. Even though no change in the molecular weight of control peptides ("light" (L) peptides) was produced, the reaction was allowed to proceed in parallel to the "heavy" (H) labelling reaction in order to avoid any possible source of bias. After labelling, to inactivate trypsin and avoid the phenomenon of back-exchange, samples were heated for 1 h at 56 °C and boiled for 10 min at 100 °C. Labelled samples were mixed in a 1:1 ratio as follows: **A**-4(H):**A**-1(L); **A**-5(H):**A**-4(L); **B**-2(H):**B**-4(L); **B**-1(H):**B**-2(L). This arrangement allowed the relative comparison of proteomes isolated from CysNO-treated cells *versus* untreated cells and CysNO-treated cells *versus* CysNO minus ascorbate-treated cells, in duplicate analysis with forward/reverse labeling. Mixed samples were purified by strong cation exchange (SCX) StageTips (*42*). Peptide mixtures were diluted with 1.5 mL of 80% acetonitrile / 0.5% formic acid (solution SCX-a) and loaded onto a 200 µL micropipette tip stacked with one layer of a strong cation exchange resin (Empore extraction disks, Sigma) previously conditioned with 20 µL of solution SCX-b (20% acetonitrile / 0.5% formic acid) and 20 µL of solution SCX-a. After two washing steps (20 µL of solution SCX-a, 20 µL of solution SCX-b), elution of tryptic peptides was achieved by adding 7 µL of 500 mM ammonium acetate / 20% acetonitrile (solution E). The eluate was dried and resuspended in 15 µL 0.1% formic acid / 2% acetonitrile. A 5 µL aliquot of each sample was subjected to nanoLC-MS/MS analysis.

CysNO treated neuronal extracts (200µM CysNO)

Exp 3
C7. 200µM Cys
C8. 200µM CysNO
C9. 200µM CysNO without ascorbate

Exp 4
E1. 200µM Cys
E2. 200µM CysNO

E3. 200µM CysNO without ascorbate

Beads thawed at 4 °C, centrifuged at 4000 rpm 1 min RT. Supernatant was removed and digested at 37 °C with 300ng of trypsin proteomics grade (Sigma) in 100 µL of 100 mM TEAB buffer, pH 8.5 (buffer C). Following tryptic digestion, the supernatants were recovered and the beads were washed three times with 20 mM TEAB in 50% MeOH (v/v) (buffer D). The washes and the first supernatant of each sample were pooled, dried and resuspended in 100 µL of buffer C (samples: SNO-proteins). Proteins were reduced further by adding 10 µL of 100 mM DTT (1h at 37 °C) and residual free cysteines were alkylated by adding 12 µL of 200 mM iodoacetamide. After quenching the reaction with additional 2 µL of 100 mM DTT, complete overnight digestion was achieved by adding a new 300 ng aliquot of trypsin. Samples were labelled according to the standard dimethyl labelling procedure (*43*). Briefly, samples were subjected to reductive amination by adding 4 µL of 0.6 M sodium cyanoborohydride and 4 µL of either formaldehyde (4% w/v, "light" label) or formaldehyde-d_2 (4% w/v, "medium" label). Samples were labelled as "light" (L) or "medium" (M) and mixed in pairs according to the Table A.

Table A: labelling scheme for dimethyl labelling experiment and generation of M:L pairs

Sample	Label	M:L pairs
C-7. NUC cys	L	80 µL of C-7 (L) + 80 µL of C-8 (M)
C-8. NUC CysNO	M	
C-9. NUC CysNO - asc	L	80 µL of C-9 (L) + 80 µL of C-8 (M)
E-1. NUC cys	L	80 µL of E-1 (L) + 80 µL of E-2 (M)
E-2. NUC CysNO	M	
E-3. NUC CysNO - asc	L	80 µL of E-3 (L) + 80 µL of E-2 (M)

Digest pairs were diluted to 2.4 mL with SCX-a solution and purified by SCX StageTips as described above. The six eluates were evaporated and peptides resuspended in 12 µL 0.1% formic acid / 2% acetonitrile. A 4 µL aliquot of each sample was subjected to nanoLC-MS/MS analysis with technical duplicates (2 injections per sample).

Exp 5

Nuclear extracts

1. 200µM Cys

2. 200µM CysNO

Cytoplasmic extracts

3. 200µM Cys

4. 200μM CysNO

SNO-proteins were isolated as described in Experiment 1. Digested proteins were prepared and labelled by O^{18} as described above, with minor modifications in starting amounts of samples subjected to isotopic labelling. As before, the volume of the supernatant + evaporated washes recovered from on-beads digestion was 100 μL. Starting amounts for the "heavy" labelling reaction were: 45 μL for samples 1 and 2; 25 μL for samples 3 and 5; 2 x 25 μL for sample 4. Exactly the same amount for each of the five samples was taken for the "light" labelling reaction.

Labelled samples were mixed in a 1:1 ratio as follows: 1(H):2(L); 1(L):2(H); 4(H):3(L); 3(H):4(L). Mixed samples were purified by strong cation exchange (SCX) StageTips as described in Exp 1. Because of the higher amount of protein sample recovered in this experiment, sample fractionation at the peptide level could be achieved (4 fractions). Thus, after tip conditioning, sample loading and washing, stepwise elution of tryptic peptides was achieved by sequential addition of 7 μL of four solutions, all containing 20% acetonitrile, of increasing ionic strength and pH: (i) 60 mM ammonium acetate, 0.5% formic acid; (ii) 120 mM ammonium acetate, 0.5% formic acid; (iii) 250 mM ammonium acetate, 0.5% formic acid; (iv) 500 mM ammonium acetate. The four SCX fractions were evaporated by vacuum centrifugation and resuspended in 8 μL of 0.1% formic acid / 2% acetonitrile. A 6 μL aliquot of each fraction (4 fractions x 6 H:L pairs) was subjected to nanoLC-MS/MS analysis.

SNO-site identification

To elute formerly cys-nitrosylated peptides still covalently attached to the beads after on-bead digestion of SNO-proteins, 100 μL of buffer B were added to each sample, followed by the addition of 10 μL of 100 mM DTT (incubation for 1 h at 37 °C). Alkylation of released cysteines was achieved by adding 10 μL of 200 mM iodoacetamide (1h at 37 °C in the dark). The supernatants were recovered, and the beads were washed with 50 μL of buffer B. Supernatants and their respective washes were pooled and evaporated in a vacuum centrifuge (samples: **SNO-peptides**). For a qualitative analysis of putative nitrosylation sites, SNO-peptides from the evaporated extracts were dissolved in 200 μL of solution SCX-a, purified by SCX StageTips as described, evaporated to dryness and reconstituted in 10 μL of 0.1% formic acid / 2% acetonitrile. A 5 μL aliquot of the pooled sample was subjected to nanoLC-MS/MS analysis. Peptides detected in the CysNO dataset of experiment 5 were assigned to proteins present in the SNO-protein dataset (biological n of ≥3). Of note, shared peptides that were detected in both Cys and CysNO conditions were also included in our combined dataset (**Table S13**).

Protein identification of total inputs in neuronal extracts

Neuronal nuclear protein extracts (50 μg) were precipitated by adding cold acetone (4:1 v/v) and

incubating the solution for 1 h at -20 °C. The pellet was solubilized in 50 µL of 5% sodium deoxycholate (DOC) containing 60 mM tris buffer (pH 8.8). Cysteine alkylation was achieved by adding sequential aliquots of, respectively, 5 µL of 100 mM DTT (1 h incubation at 37 °C), 6 µL of 200 mM iodoacetamide (1 h incubation at 37 °C), 1 µL of 100 mM DTT (20 min incubation at 37 °C). Solution volume was brought to 500 µL by adding 20 mM tris buffer. Overnight protein digestion was allowed to proceed at 37 °C after adding sequencing grade trypsin (Sigma, 1:100 w/w). The enzymatic reaction was quenched by the addition of 50 µL of 5% trifluroacetic acid, which served also for precipitating the DOC detergent. After spinning down the precipitate on a bench centrifuge, 200 µL of the supernatant were removed and purified on RP StageTips as described in previous paragraphs. Finally, the purified peptide mixture was fractionated on SCX StageTips as described above. Stepwise elution of tryptic peptides from SCX StageTips was achieved by sequential addition of 20 µL of seven solutions, all containing 20% acetonitrile, of increasing ionic strength and pH: (i) 50 mM ammonium acetate, 0.5% acetic acid; (ii) 75 mM ammonium acetate, 0.5% acetic acid; (iii) 100 mM ammonium acetate, 0.5% acetic acid; (iv) 150 mM ammonium acetate, 0.5% acetic acid; (v) 250 mM ammonium acetate, 0.5% acetic acid; (vi) 350 mM ammonium acetate, 0.5% acetic acid; (vii) 500 mM ammonium acetate. Fractions were evaporated by vacuum centrifugation and resuspended in 15 µL of 0.1% formic acid / 2% acetonitrile. A 2 µL aliquot of each fraction was subjected to nanoLC-MS/MS analysis using a long elution gradient (see below).

nanoLC-MS/MS analysis for neuronal extracts

Chromatography was performed on an **Easy LC 1000 nanoscale liquid chromatography (nanoLC) system** (Thermo Fisher Scientific, Odense, Denmark). The analytical nanoLC column was a pulled fused silica capillary, 75 µm i.d., in-house packed to a length of 10 cm with 3 µm C18 silica particles from Dr. Maisch (Entringen, Germany). The peptide mixtures were loaded at 500 nL/min directly onto the analytical column. A binary gradient was used for peptide elution. Mobile phase A was 0.1% formic acid, 2% acetonitrile, whereas mobile phase B was 0.1% formic acid, 80% acetonitrile. Peptides were separated by a gradient elution at a 300 nL/min flow rate, ramping from 5% B to 35% B in 60 min (50 min for SNO-peptides, 120 min for nuclear extracts), and from 35% B to 100% B in additional 15 min; after 5 min at 100% B, the column was re-equilibrated at 2% B for 10 min before the following injection. MS detection was performed on a quadrupole-orbitrap mass spectrometer **Q-Exactive (Thermo Fisher Scientific, Bremen, Germany)** operating in positive ion mode, with nanoelectrospray (nESI) potential at 1800 V applied on the column front-end via a tee piece. Data-dependent acquisition was performed by using a top-12 method (top-8 for SNO-peptide), where the twelve most abundant ions were automatically selected for HCD fragmentation at normalized collision energy of 25%. Resolution (FWHM), AGC target and maximum injection time (ms) for full MS and MS/MS were 70,000/17,500, 1e6/1e5, 20/60, respectively. MS/MS parameters for detection of SNO-peptides were: resolution 35,000; AGC target 2e5, max injection time 120 ms. MS full scan

range was 350-1800 m/z. Mass window for precursor ion isolation was 1.6 m/z. Ion threshold for triggering MS/MS events was 5e4. Dynamic exclusion was 30 s.

Data analysis for neuronal extracts

Protein identification and quantification was achieved in Proteome Discoverer 1.4 (Thermo Fisher Scientific, Bremen, Germany), using Sequest as search engine and the RATTUS proteome sequence database (http://www.ebi.ac.uk/uniprot) accessed on March 2015. The database was merged with a list of common contaminants named "Common Repository of Adventitious Proteins" retrieved from The Global Proteome Machine website (http://www.thegpm.org/crap/index.html). In total, 27,927 entries were searched. The following general search parameters were used: MS tolerance 15 ppm; MS/MS tolerance 0.02 Da; enzyme trypsin; max. missed cleavages 2; variable modification: oxidised methionine. Additionally, the following search parameters were used, depending on Experiment number: Exp 1 and 2) variable modification: C-terminal ^{18}O labelling; fixed modification: methyl thio-cysteine (MMTS); Exp. 3 and 4) variable modifications: N-ethylmaleimide-cysteine (NEM), scarbamidomethyl-cysteine (CAM); fixed modifications (in two parallel searches): (a) N-ter dimethyl (light); dimethyl-lysine (light); (b) N-ter dimethyl (medium); dimethyl-lysine (medium). Exp. 5) variable modification: C-terminal ^{18}O labelling; fixed modification: N-ethylmaleimide-cysteine (NEM); For SNO-peptide searches, the following additional parameters were used: Exp. 1 and 5) fixed modification: carbamidomethyl-cysteine (CAM). False discovery rate estimation was performed in Proteome Discoverer using the Target-decoy validator node. Minimum requirement for protein ID for every experiment was 2 peptides at 95% confidence, whereas for SNO-peptide identification peptide confidence threshold was set to 99%.

Hit criteria for SNO-Ps

In order to be considered a target for S-nitrosylation, proteins detected from mass spectrometry had to be enriched ≥ 2 fold in CysNO samples versus control in 3 experiments and not enriched ≥ 2 fold in any control. Sodium ascorbate is required as a reducing agent for S-nitrosothiols, therefore samples in which sodium ascorbate were omitted were used as negative controls (See Table S2).

Motif-X analysis

Motif-X (motif-x.med.harvard.edu) (*44, 45*). Foreground: SNO-peptides associated with S-nitrosylated protein hits. Settings: Extended from IPI Rat Proteome, central character: C, width: 21, significance: 0.000001. Background: IPI Rat Proteome, background central character: C.

References

1. P. Anand, J. S. Stamler, Enzymatic mechanisms regulating protein S-nitrosylation: implications in health and disease. *J Mol Med (Berl)* **90**, 233-244 (2012).
2. D. T. Hess, A. Matsumoto, S. O. Kim, H. E. Marshall, J. S. Stamler, Protein S-nitrosylation: purview and parameters. *Nat Rev Mol Cell Biol* **6**, 150-166 (2005).
3. N. Gould, P. T. Doulias, M. Tenopoulou, K. Raju, H. Ischiropoulos, Regulation of protein function and signaling by reversible cysteine S-nitrosylation. *J Biol Chem* **288**, 26473-26479 (2013).
4. A. Nott, P. M. Watson, J. D. Robinson, L. Crepaldi, A. Riccio, S-Nitrosylation of histone deacetylase 2 induces chromatin remodelling in neurons. *Nature* **455**, 411-415 (2008).
5. M. D. Kornberg *et al.*, GAPDH mediates nitrosylation of nuclear proteins. *Nat Cell Biol* **12**, 1094-1100 (2010).
6. S. Okamoto *et al.*, S-nitrosylation-mediated redox transcriptional switch modulates neurogenesis and neuronal cell death. *Cell Rep* **8**, 217-228 (2014).
7. D. S. Bredt, S. H. Snyder, Transient nitric oxide synthase neurons in embryonic cerebral cortical plate, sensory ganglia, and olfactory epithelium. *Neuron* **13**, 301-313 (1994).
8. A. Nott *et al.*, S-nitrosylation of HDAC2 regulates the expression of the chromatin-remodeling factor Brm during radial neuron migration. *Proc Natl Acad Sci U S A* **110**, 3113-3118 (2013).
9. J. Graff *et al.*, Epigenetic priming of memory updating during reconsolidation to attenuate remote fear memories. *Cell* **156**, 261-276 (2014).
10. M. R. Hara *et al.*, S-nitrosylated GAPDH initiates apoptotic cell death by nuclear translocation following Siah1 binding. *Nat Cell Biol* **7**, 665-674 (2005).
11. S. D. Ryan *et al.*, Isogenic human iPSC Parkinson's model shows nitrosative stress-induced dysfunction in MEF2-PGC1alpha transcription. *Cell* **155**, 1351-1364 (2013).
12. P. T. Doulias, M. Tenopoulou, J. L. Greene, K. Raju, H. Ischiropoulos, Nitric oxide regulates mitochondrial fatty acid metabolism through reversible protein S-nitrosylation. *Sci Signal* **6**, rs1 (2013).
13. K. Raju *et al.*, Regulation of brain glutamate metabolism by nitric oxide and S-nitrosylation. *Sci Signal* **8**, ra68 (2015).
14. U. Seneviratne *et al.*, S-nitrosation of proteins relevant to Alzheimer's disease during early stages of neurodegeneration. *Proc Natl Acad Sci U S A* **113**, 4152-4157 (2016).
15. M. T. Forrester *et al.*, Proteomic analysis of S-nitrosylation and denitrosylation by resin-assisted capture. *Nat Biotechnol* **27**, 557-559 (2009).
16. B. E. Lonze, D. D. Ginty, Function and regulation of CREB family transcription factors in the nervous system. *Neuron* **35**, 605-623 (2002).
17. A. Riccio *et al.*, A nitric oxide signaling pathway controls CREB-mediated gene expression in neurons. *Mol Cell* **21**, 283-294 (2006).
18. S. R. Jaffrey, S. H. Snyder, The biotin switch method for the detection of S-nitrosylated proteins. *Sci STKE* **2001**, pl1 (2001).
19. Y. Xue *et al.*, NURD, a novel complex with both ATP-dependent chromatin-remodeling and histone deacetylase activities. *Mol Cell* **2**, 851-861 (1998).
20. A. Kuzmichev, K. Nishioka, H. Erdjument-Bromage, P. Tempst, D. Reinberg, Histone methyltransferase activity associated with a human multiprotein complex containing the Enhancer of Zeste protein. *Genes Dev* **16**, 2893-2905 (2002).
21. J. Nitarska *et al.*, A Functional Switch of NuRD Chromatin Remodeling Complex Subunits Regulates Mouse Cortical Development. *Cell Rep* **17**, 1683-1698 (2016).

22. J. S. Stamler, E. J. Toone, S. A. Lipton, N. J. Sucher, (S)NO signals: translocation, regulation, and a consensus motif. *Neuron* **18**, 691-696 (1997).

23. S. M. Marino, V. N. Gladyshev, Structural analysis of cysteine S-nitrosylation: a modified acid-based motif and the emerging role of trans-nitrosylation. *J Mol Biol* **395**, 844-859 (2010).

24. M. J. Kohr *et al.*, Characterization of potential S-nitrosylation sites in the myocardium. *Am J Physiol Heart Circ Physiol* **300**, H1327-1335 (2011).

25. N. V. Murzina *et al.*, Structural basis for the recognition of histone H4 by the histone-chaperone RbAp46. *Structure* **16**, 1077-1085 (2008).

26. D. Carrel *et al.*, Nitric oxide synthase 1 adaptor protein, a protein implicated in schizophrenia, controls radial migration of cortical neurons. *Biol Psychiatry* **77**, 969-978 (2015).

27. S. B. Lee, C. K. Kim, K. H. Lee, J. Y. Ahn, S-nitrosylation of B23/nucleophosmin by GAPDH protects cells from the SIAH1-GAPDH death cascade. *J Cell Biol* **199**, 65-76 (2012).

28. H. S. Chung *et al.*, Dual Labeling Biotin Switch Assay to Reduce Bias Derived From Different Cysteine Subpopulations: A Method to Maximize S-Nitrosylation Detection. *Circ Res* **117**, 846-857 (2015).

29. Q. Luo *et al.*, Mechanism of CREB recognition and coactivation by the CREB-regulated transcriptional coactivator CRTC2. *Proc Natl Acad Sci U S A* **109**, 20865-20870 (2012).

30. Q. Lin *et al.*, MicroRNA-mediated disruption of dendritogenesis during a critical period of development influences cognitive capacity later in life. *Proc Natl Acad Sci U S A* **114**, 9188-9193 (2017).

31. K. Wolhuter *et al.*, Evidence against Stable Protein S-Nitrosylation as a Widespread Mechanism of Post-translational Regulation. *Mol Cell* **69**, 438-450 e435 (2018).

32. Y. T. Wang, S. C. Piyankarage, D. L. Williams, G. R. Thatcher, Proteomic profiling of nitrosative stress: protein S-oxidation accompanies S-nitrosylation. *ACS Chem Biol* **9**, 821-830 (2014).

33. M. Chaki *et al.*, Identification of nuclear target proteins for S-nitrosylation in pathogen-treated Arabidopsis thaliana cell cultures. *Plant Sci* **238**, 115-126 (2015).

34. J. Hu *et al.*, Nitric Oxide Regulates Protein Methylation during Stress Responses in Plants. *Mol Cell* **67**, 702-710 e704 (2017).

35. S. L. Berger, P. Sassone-Corsi, Metabolic Signaling to Chromatin. *Cold Spring Harb Perspect Biol* **8**, (2016).

36. J. Jia *et al.*, Target-selective protein S-nitrosylation by sequence motif recognition. *Cell* **159**, 623-634 (2014).

37. N. J. Fowler, C. F. Blanford, S. P. de Visser, J. Warwicker, Features of reactive cysteines discovered through computation: from kinase inhibition to enrichment around protein degrons. *Sci Rep* **7**, 16338 (2017).

38. M. T. Forrester, M. W. Foster, J. S. Stamler, Assessment and application of the biotin switch technique for examining protein S-nitrosylation under conditions of pharmacologically induced oxidative stress. *J Biol Chem* **282**, 13977-13983 (2007).

39. M. T. Forrester, M. W. Foster, M. Benhar, J. S. Stamler, Detection of protein S-nitrosylation with the biotin-switch technique. *Free Radic Biol Med* **46**, 119-126 (2009).

40. J. A. Cook *et al.*, Convenient colorimetric and fluorometric assays for S-nitrosothiols. *Anal Biochem* **238**, 150-158 (1996).

41.   F. Bernaudo *et al.*, Validation of a Novel Shotgun Proteomic Workflow for the Discovery of Protein-Protein Interactions: Focus on ZNF521. *Journal of Proteome Research* **14**, 1888-1899 (2015).

42.   J. Rappsilber, M. Mann, Y. Ishihama, Protocol for micro-purification, enrichment, pre-fractionation and storage of peptides for proteomics using StageTips. *Nat Protoc* **2**, 1896-1906 (2007).

43.   P. J. Boersema, R. Raijmakers, S. Lemeer, S. Mohammed, A. J. Heck, Multiplex peptide stable isotope dimethyl labeling for quantitative proteomics. *Nat Protoc* **4**, 484-494 (2009).

44.   M. F. Chou, D. Schwartz, Biological sequence motif discovery using motif-x. *Curr Protoc Bioinformatics* **Chapter 13**, Unit 13 15-24 (2011).

45.   D. Schwartz, S. P. Gygi, An iterative statistical approach to the identification of protein phosphorylation motifs from large-scale data sets. *Nat Biotechnol* **23**, 1391-1398 (2005).

46.   E. W. Deutsch *et al.*, The ProteomeXchange consortium in 2017: supporting the cultural change in proteomics public data deposition. *Nucleic Acids Res* **45**, D1100-D1106 (2017).

47.   J. A. Vizcaino *et al.*, 2016 update of the PRIDE database and its related tools. *Nucleic Acids Res* **44**, 11033 (2016).

Author Contributions

A.R., J.G.S. designed research, J.G.S., S.G.A., C.A., C.G., M.G. performed research, J.G.S., S.G.A., M.G. analysed data, J.G.S., A.R. wrote the manuscript.
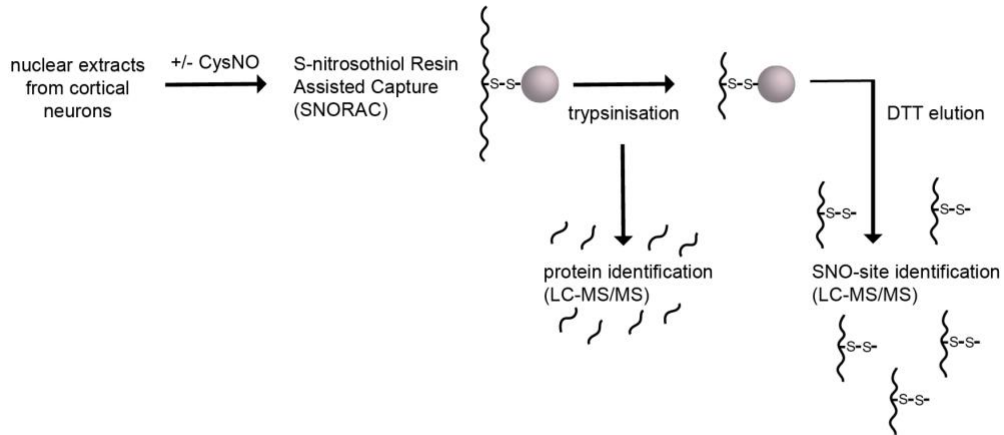
Competing Interests

The authors declare that they have no competing interests.
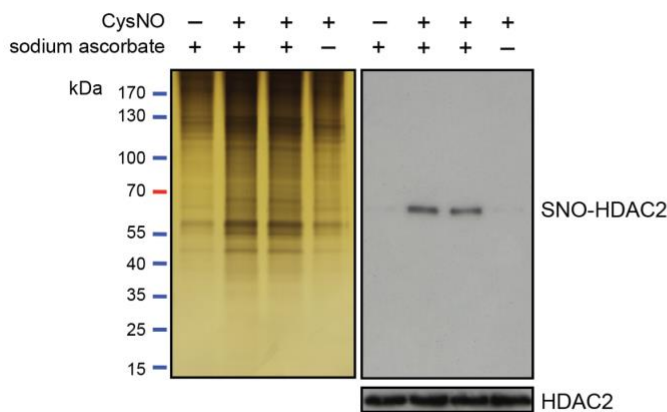
Data and Materials availability

The mass spectrometry proteomics data have been deposited to the ProteomeXchange Consortium (*46*) via the PRIDE (*47*) partner repository with the dataset identifier PXD009071.

Figure 1

A

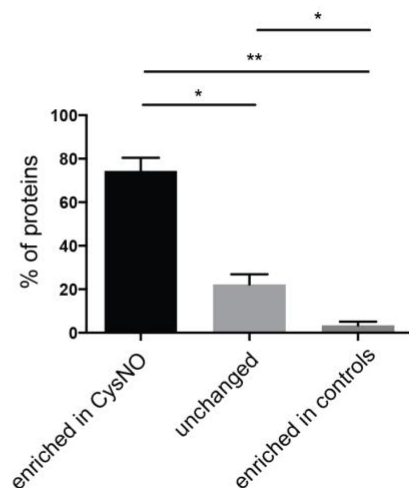**B**   **C**

Fig. 1. Identification of S-nitrosylated nuclear proteins using SNORAC. (A) Nuclear extracts from E17 cortical neurons were treated with CysNO and S-nitrosylated proteins captured using SNORAC. Resin-bound proteins were trypsinised and eluted fragments analysed by quantitative mass spectrometry to identify proteins enriched in CysNO-treated groups. A second elution step was carried out using DTT, releasing fragments containing the previously S-nitrosylated cysteines and allowing the identification of S-nitrosylation sites (SNO-sites). **(B)** Silver stain of proteins isolated using SNORAC, and HDAC2 western blotting on SNORAC eluates and total inputs. Sodium ascorbate is required for isolation of S-nitrosylated proteins using SNO-RAC (see **Methods**). Representative blot, n of 5 independent experiments. **(C)** Average percentage of proteins detected by

mass spectrometry as enriched in CysNO (≥ 2 fold vs control), unchanged ($< 2, > 0.5$; CysNO vs control), or enriched in controls (≤ 0.5 fold; CysNO vs control). Control groups constitute Cys only and CysNO without ascorbate. Data from 5 independent experiments are shown as mean +/- SEM. *$p<0.05$,**$p<0.01$ (Row means one-way ANOVA, Tukey).

Figure 2
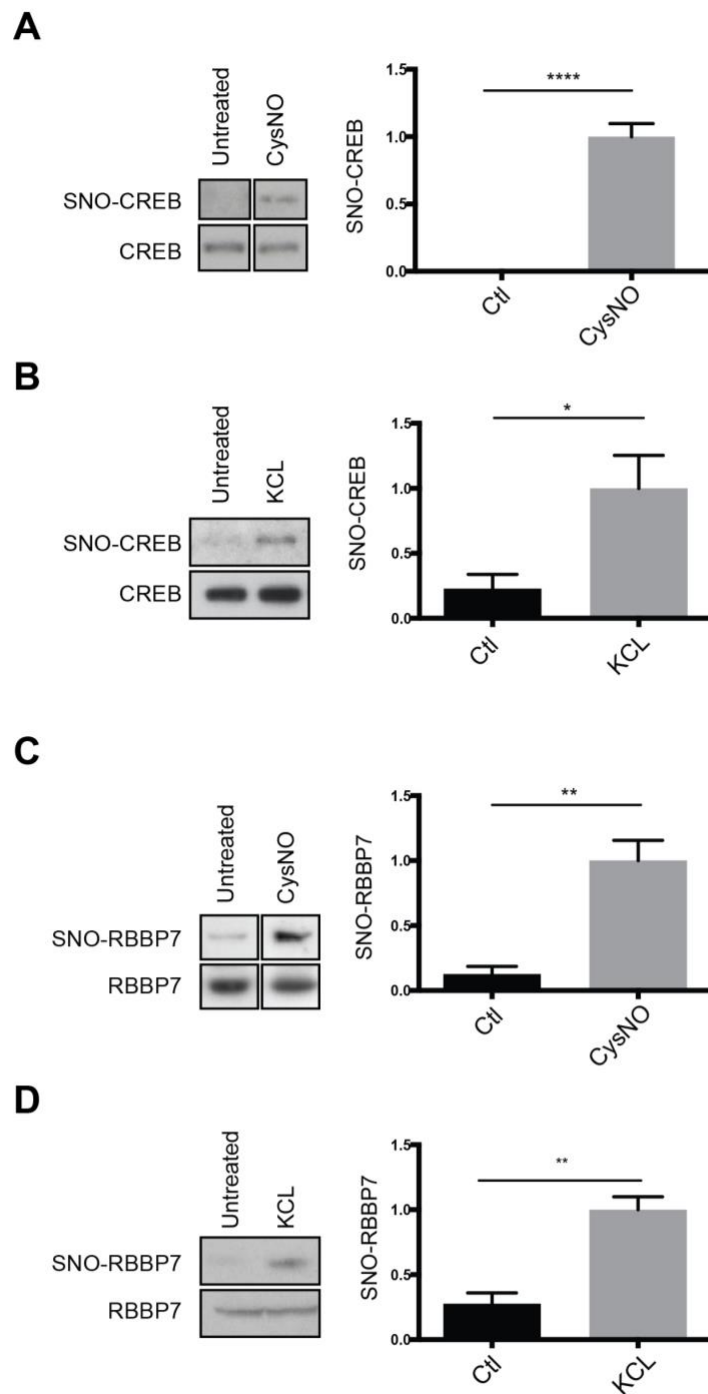
Fig. 2. S-nitrosylation of CREB and RBBP7 in cortical neurons. (A) E17 rat cortical neurons were cultured for 4 days and treated with CysNO (200 μM for 20 mins). S-nitrosylated proteins were isolated by SNORAC (n=2 independent experiments) or biotin switch (n=2 independent experiments). Non-contiguous lanes from the same experiment and blot are shown side by side. **(B)** Cortical neurons were exposed to KCL (50 mM for 20 mins) and S-nitrosylated proteins were isolated by SNORAC

(n=2 independent experiments) or biotin switch (n=1 independent experiment). Data combined for analysis. **(C)** Neurons were were treated with CysNO (200 μM for 20 mins) and S-nitrosylated proteins isolated by biotin switch (n=4 independent experiments). Non-contiguous lanes from the same experiment and blot are shown side by side. **(D)** Cortical neurons (4 days in vitro) were exposed to KCL and S-nitrosylated proteins isolated by biotin switch (n=2 independent experiments using KCL 30 mins, n=1 independent experiment for KCL 20 mins. Data combined for analysis). For both CREB and RBBP7, isolated proteins were separated by SDS-PAGE and western blot analysis was carried out using antibodies against CREB or RBBP7. Densitometry analysis on the western blots was performed using ImageJ. SNO-protein signals were first adjusted according to inputs. All data are shown as mean +/- SEM (Unpaired t-test, *P=<0.05, **P=<0.01, ***P=<0.0001).

Figure 3

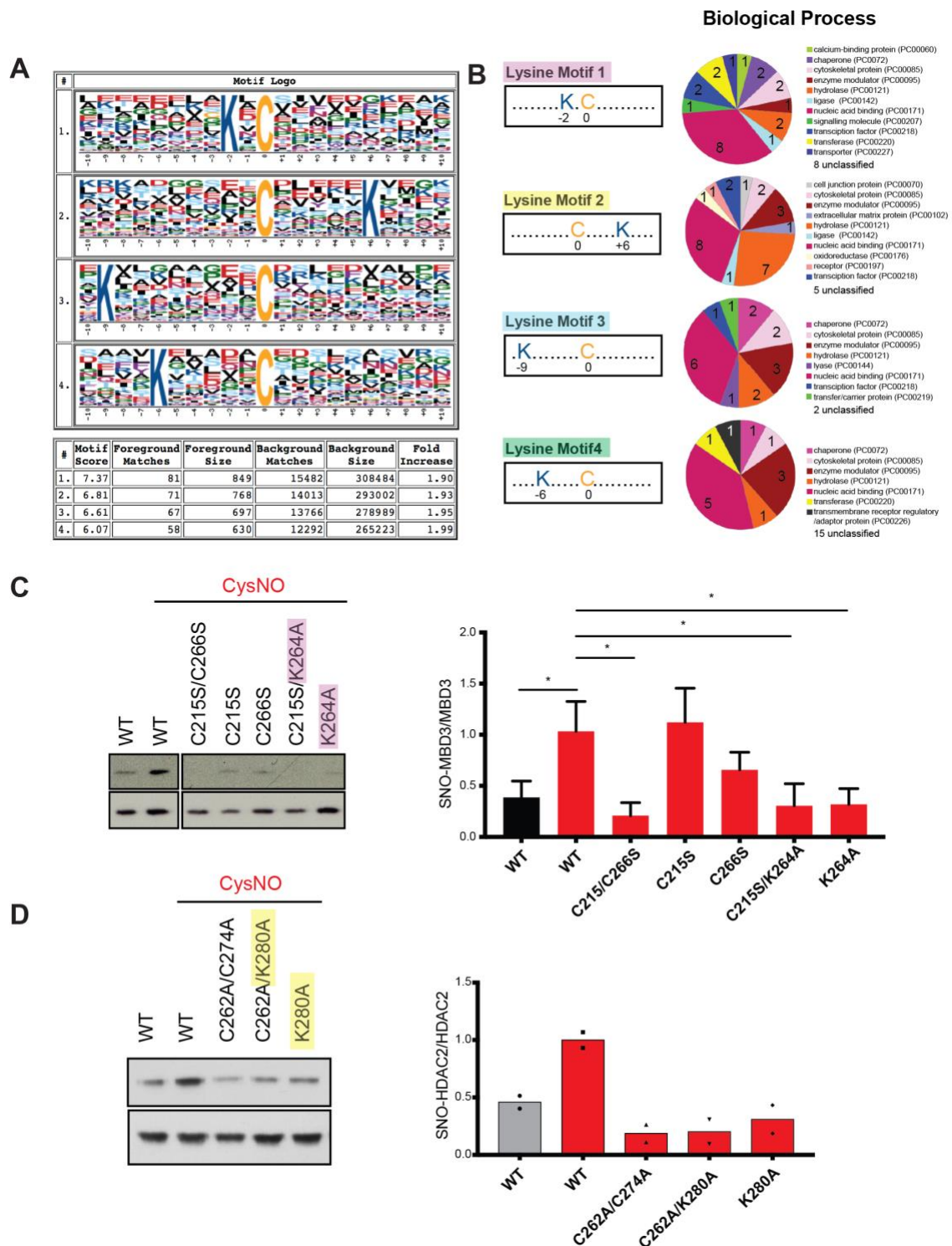**Fig. 3. Lysine motifs regulate S-nitrosylation (A)** Cysteine-containing peptides associated with nuclear SNO-proteins were subjected to SNO-site analysis using Motif-X (see Methods) and the IPI rat proteome, as background. Graphical representation of the motifs; the size of each letters refers the probability of occurrence of that amino acid in cysteine containing peptides. Summary table displayed

for clarity. Full size letters (as for cysteine; C, lysine; K) indicate their recurrence in each motif. **(B)** Gene ontology (GO) analysis of proteins that contain either lysine motif 1, 2, 3 or 4 only around their identified S-nitrosylated cysteines. Analysis carried out using PANTHER Functional Classification for Biological Process, Version 13.1 released 2018-02-03, pantherdb.org. **(C)** SNO-motif mutational analysis of MBD3. Western blotting and densitometry analysis of HEK293T cells transfected with vectors expressing myc-tagged wild type MBD3 (WT), MBD3 cysteine-to-serine mutants (C215S and C266S), MBD3 lysine 264-to-alanine mutant (K264A) and cysteine and alanine combined mutant (C215S/K264A). 24h after transfection, cells were exposed to Cys or CysNO (200µM for 20 mins) and subjected to the biotin switch assay. n=4 independent experiments. Data are shown as mean +/- SEM (One-way ANOVA, compared to control column 'WT + CysNO', Fisher's LSD, *p≤0.05). Non-contiguous lanes from the same experiment and blot are shown side by side, as indicated by the separation evident in the figure. **(D)** SNO-motif mutational analysis of HDAC2. Vectors expressing HA-tagged wild type HDAC2 (WT), HDAC2 cysteine-to-alanine nitrosomutant (C264A/C272A), HDAC2 lysine 280-to-alanine mutant (K280A) and cysteine and alanine combined mutant (C264A/K280A). 48h after transfection, cells were exposed to Cys or CysNO (200µM for 20 mins) and subjected to the biotin switch assay. n=2 independent experiments.

Figure 4

Fig. 4. SNO-site identification for CREB and RBBP7. (A) Domain structure of CREB. Q1= glutamine rich region 1, α= alpha domain, KID= kinase inducible domain, Q2= glutamine rich region 2, bZIP= bZIP domain. CREB1 cysteines are annotated (C90, C300, C310, C337). Phosphorylated serines (S133, S142, S143) are shown along with their respective kinases (protein kinase A (PKA), protein kinase C (PKC) and Ca2+/calmodulin-dependent protein kinase II (CaMKII)) **(B)** Vectors expressing myc-tagged wild type CREB (WT) or CREB cysteine-to-serine mutants were transfected

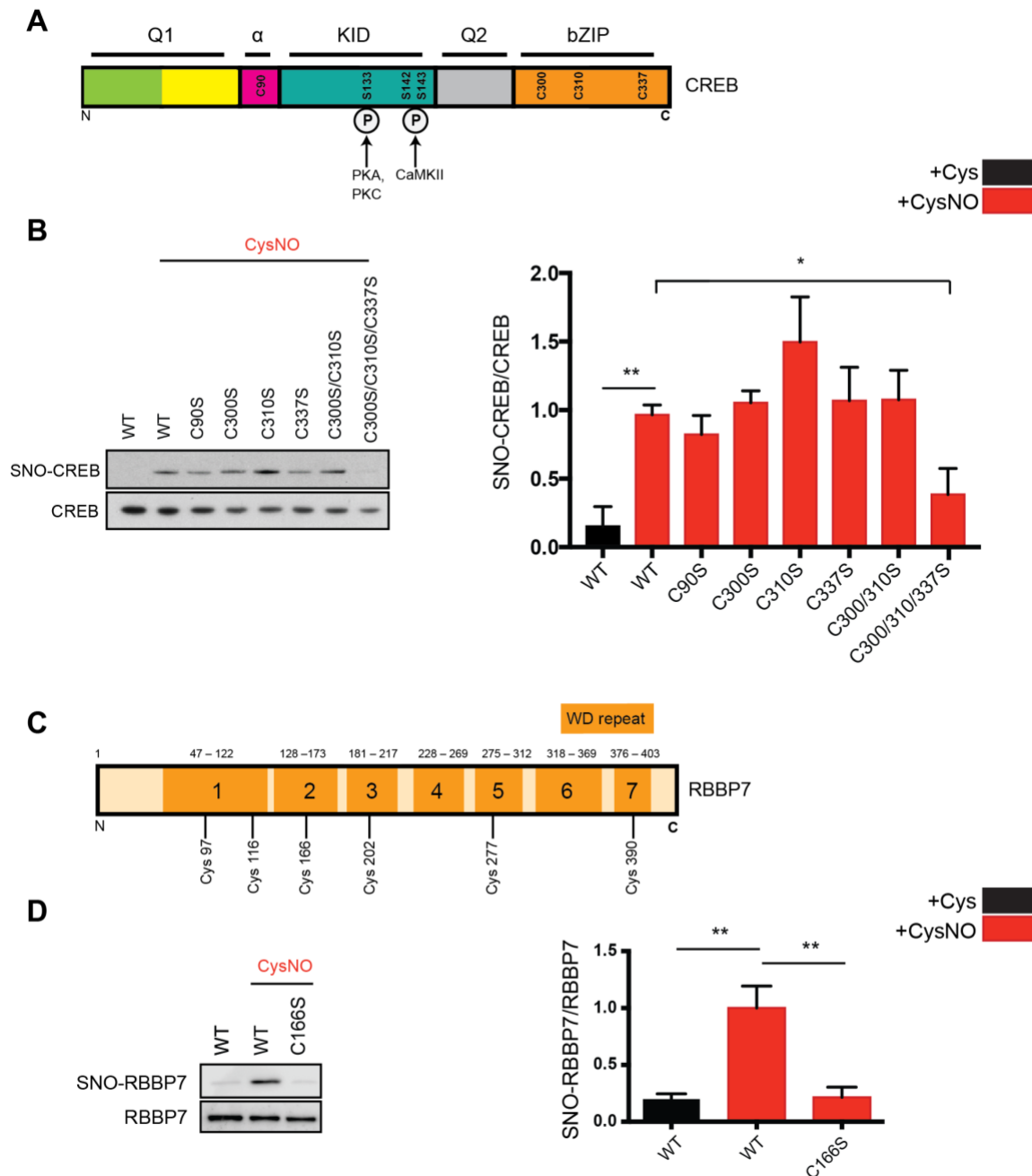into HEK293T cells, and after 48h, cell lysates were exposed to Cys or CysNO (500µM for 20 mins) and subjected to the biotin switch assay. n=3 independent experiments. **(C)** RBBP7 contains 7 WD-repeat domains, composed of short motifs of approximately 40 amino acids and ending in a typrophan-aspartic acid dipeptide. **(D)** Vectors expressing myc-tagged wild type RBBP7 (WT) or RBBP7 cysteine 166 to serine mutant (C166S) were transfected into HEK293T cells. After 48h, cells were treated with Cys or CysNO (500µM for 20 mins) and lysates were subjected to the biotin switch assay. n=3 independent experiments. Isolated proteins and total inputs were separated by SDS-PAGE then immunoblotted using an antibody against myc. Densitometry analysis carried out using ImageJ. SNO-signals were normalised to total inputs and expressed as fold change relative to WT + CysNO. All data are shown as mean +/- SEM. One-way ANOVA, compared to 'WT + CysNO' column, Fisher's LSD; $*p \leq 0.05$, $**p < 0.01$.

Figure 5
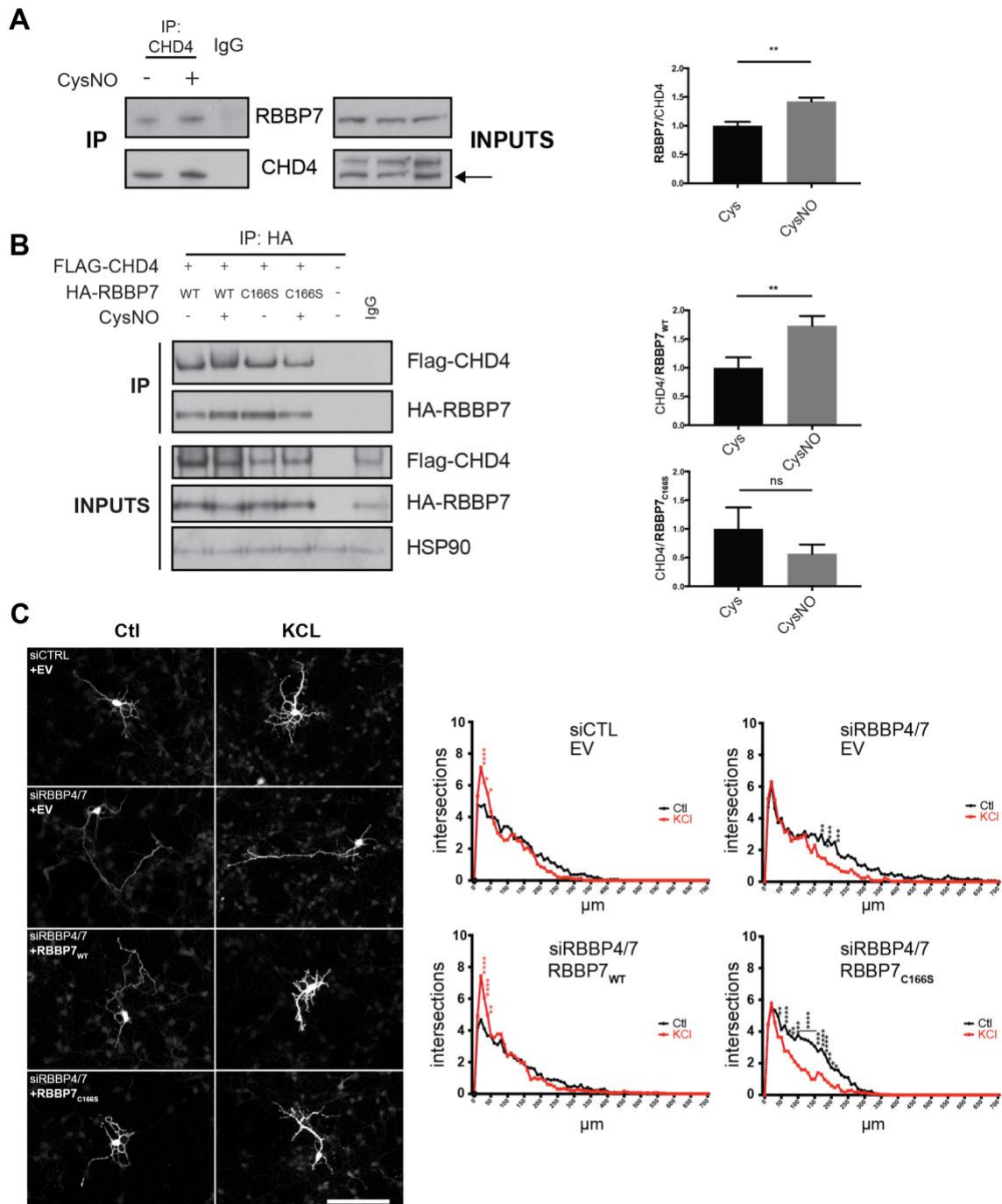
Fig. 5. S-nitrosylation of RBBP7 regulates dendritogenesis (A) S-nitrosylation of RBBP7 regulates the interaction with CHD4. E17 rat cortical neurons were cultured for 4 days, treated with 200μM CysNO for 20 minutes and subjected to co-immunoprecipitation using an antibody against CHD4. As a control, pooled samples (of Cys and CysNO) were subjected to immunoprecipition using an IgG antibody. Western blot analysis was carried out on eluates and inputs using indicated antibodies.

Densitometry analysis of co-immunoprecipitated RBBP7 shown in relation to co-immunoprecipitated CHD4 (n=4 independent experiments, **p<0.01, unpaired t-test). Densitometry was carried out by normalising RBBP7 pulldown signal to RBBP7 inputs, then dividing this value by the pulldown signal for CHD4. **(B)** S-nitrosylation of RBBP7 at cysteine 166 promotes the interaction with CHD4. HEK293T cells were transfected with vectors expressing Flag-mCHD4 and HA-RBBP7^{WT} or HA-RBBP7^{C166S}, treated with 200μM CysNO for 20 mins and pulldown carried out on eluates using an antibody against HA. Western blot analysis was carried out on eluates and inputs using indicated antibodies. Densitometry analysis of FLAG-CHD4 displayed in relation to HA-RBBP7, normalised to FLAG-CHD4 inputs (n= 3 independent experiments, **p<0.01, unpaired t-test). Densitometry was carried out by normalising FLAG-CHD4 pulldown signal to FLAG-CHD4 inputs, then dividing this value by the pulldown signal for HA-RBBP7. **(C)** S-nitrosylation of RBBP7 promotes dentritogenesis in cortical neurons. Control siRNA (CTL) or siRNAs targeting RBBP4 and RBBP7 (siRBBP4/7) were transfected into E15 mouse cortical neurons alongside a GFP expression vector and EV, siRNA-resistant myc-RBBP7^{WT} or myc-RBBP7^{C166S} as shown. Neurons were maintained in control conditions (Ctl) or exposed to 50mM KCl (KCl) for 2 days and immunostained for GFP. Resulting images were analysed using FIJI Sholl plugin. Maximal projections show representative neurons for each condition. Scale bar: 100μm. Summary of Sholl data analysis for each condition is shown. 3 biological replicates were carried out in which 10 neurons were analysed per experiment (30 neurons in total). Shown are mean values for number of intersections (intersections) against distance from the soma (μm). Readings were taken every 10μm. *p<0.05, **p<0.01, ***p<0.001, ****p<0.0001. Red stars indicate KCl value is significantly greater than Ctl, black stars indicate Ctl value is significantly greater than KCL. Row means two-way ANOVA with Sidak's test for multiple comparisons.

Figure S1
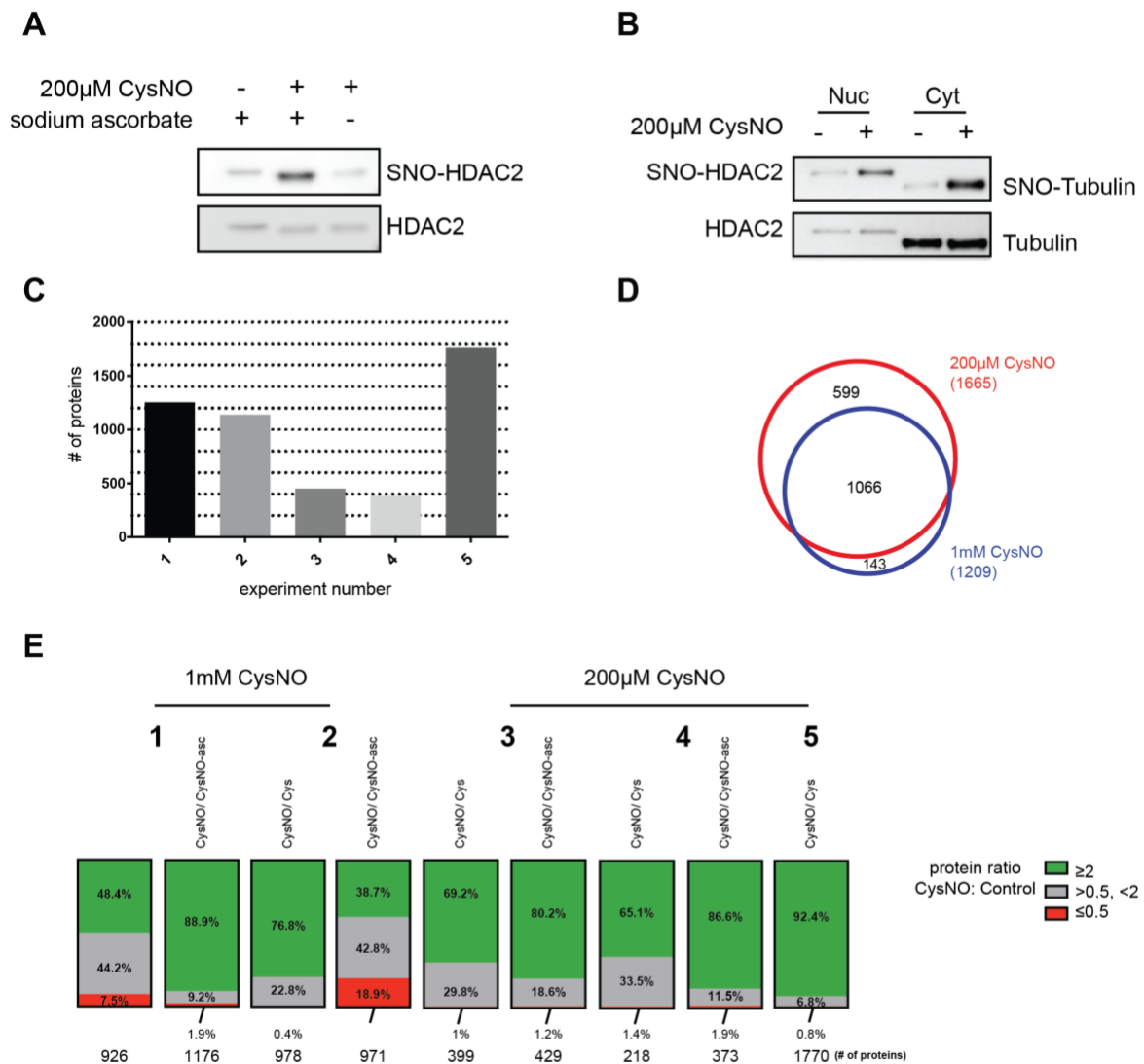
Fig. S1. SNORAC Screen Analysis. (A) Nuclear extracts from cortical neurons were treated with 200μM Cys or CysNO for 20 minutes, followed by SNORAC and western blotting of isolates and inputs for HDAC2 (n=2 independent experiments). Sodium ascorbate is required for reduction of S-nitrosothiols. **(B)** Nuclear and cytoplasmic extracts were treated with 200μM Cys or CysNO for 20 minutes, followed by western blot for HDAC2 and Tubulin (representative blot of n=3 independent experiments). **(C)** Total number of proteins detected as enriched in CysNO (≥ 2 fold) groups in each experiment. Proteins were compiled from both 'CysNO vs Cys' and 'CysNO vs CysNO w/o ascorbate' for each experiment. **(D)** Comparison of the number of proteins detected as ≥ 2 fold enriched in CysNO versus control groups, in at least 1 experiment. **(E)** Relative proportion of proteins

detected as enriched either ≥ 2 fold in CysNO groups (green), unchanged (grey) or enriched ≥ 2 fold in controls (red). CysNO concentration in experiments 1 and 2 is 1mM CysNO and 200µM in experiments 3-5.

Figure S2
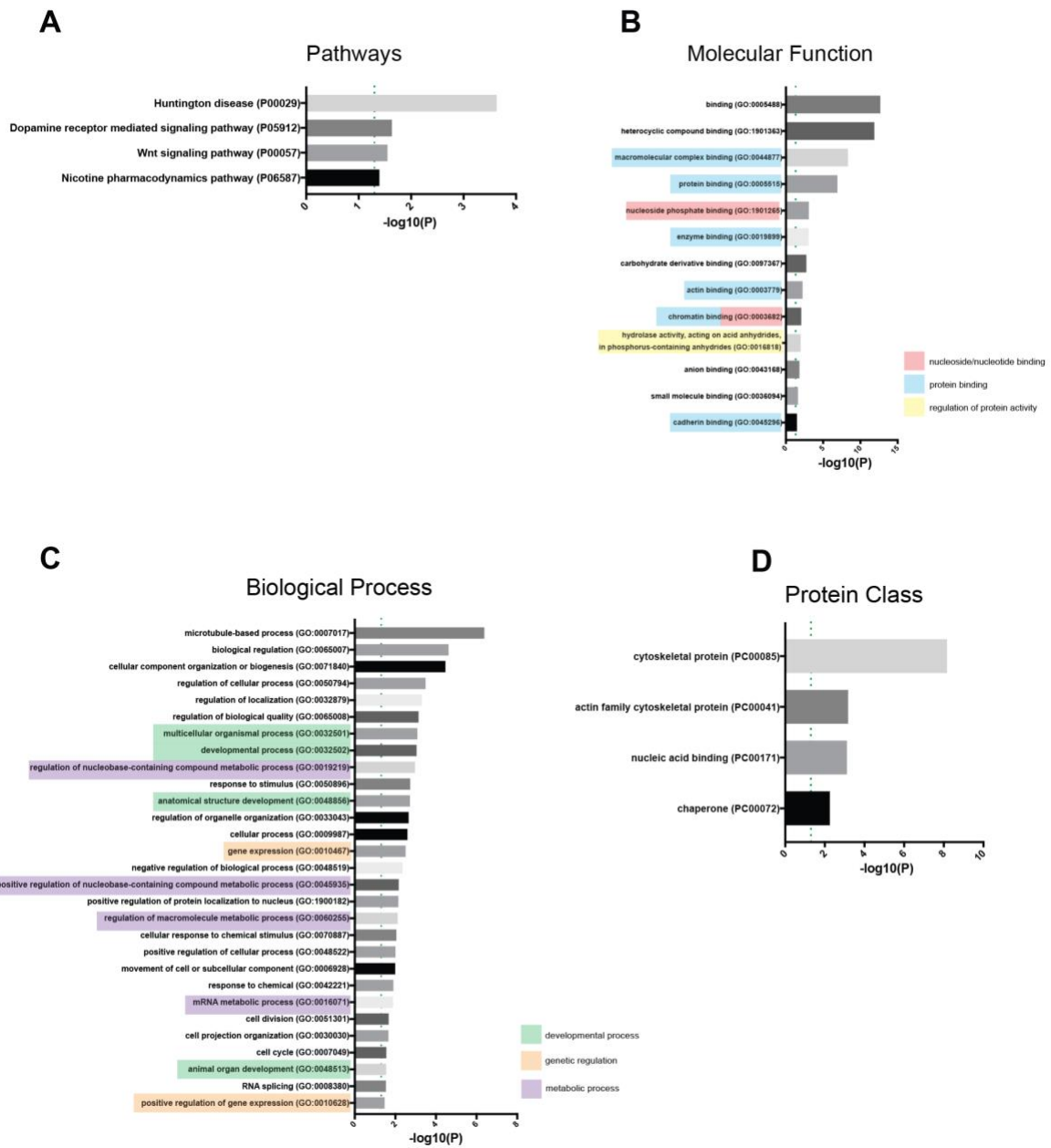
Fig. S2. PANTHER Gene Ontology Overrepresentation Analysis. Overrepresentation analysis was carried out using S-nitrosylated hits (Table S2) as the assayed dataset and our nuclear protein dataset (**Table S7**) as background. P>0.05 (-log10(P) of 1.3 and above) was considered as statistically significant; all terms displayed here reach this threshold, indicated by dashed green line. Bonferroni correction for multiple testing was carried out. Displayed are the parent terms only. Shown are overrepresented terms for Pathways (**A**), Molecular Function (**B**), Biological Process (**C**) and Protein

Class **(D).** Analysis carried out using PANTHER Overrepresentation Test (release 20170413); PANTHER version 12 Released 2017-07-10, pantherdb.org.

A

SNO-proteins
nuclear extracts

calcium-binding protein (PC00060) **2.30% (12)**
cell adhesion molecule (PC00069) **0.40% (2)**
cell junction protein (PC00070) **0.40% (2)**
chaperone (PC00072) **4.00% (21)**
cytoskeletal protein (PC00085) **11.30% (60)**
defense/immunity protein (PC00090) **0.60% (3)**
enzyme modulator (PC00095) **8.10% (43)**
extracellular matrix protein (PC00102) **0.40% (2)**
hydrolase (PC00121) **7.40% (39)**
isomerase (PC00135) **0.80% (4)**
kinase (PC00137) **2.10% (11)**
ligase (PC00142) **2.80% (15)**
lyase (PC00144) **0.80% (4)**
membrane traffic protein (PC00150) **1.30% (7)**
nucleic acid binding (PC00171) **30.20% (160)**
oxidoreductase (PC00176) **3.20% (17)**
phosphatase (PC00181) **1.30% (7)**
protease (PC00190) **1.10% (6)**
receptor (PC00197) **1.30% (7)**
signaling molecule (PC00207) **2.80% (15)**
structural protein (PC00211) **0.80% (4)**
surfactant (PC00212) **0.20% (1)**
transcription factor (PC00218) **7.50% (40)**
transfer/carrier protein (PC00219) **0.90% (5)**
transferase (PC00220) **5.70% (30)**
transmembrane receptor regulatory/adaptor protein (PC00226) **0.40% (2)**
transporter (PC00227) **2.10% (11)**

Total=530

SNO-proteins
cytoplasmic extracts

calcium-binding protein (PC00060) **2.82% (12)**
cell adhesion molecule (PC00069) **1.41% 6**
cell junction protein (PC00070) **0.47% (2)**
chaperone (PC00072) **5.40% (23)**
cytoskeletal protein (PC00085) **11.03% (47)**
defense/immunity protein (PC00090) **0.23% (1)**
enzyme modulator (PC00095) **12.68% (54)**
extracellular matrix protein (PC00102) **0.47% (2)**
hydrolase (PC00121) **9.39% (40)**
isomerase (PC00135) **1.17% (5)**
kinase (PC00137) **5.40% (23)**
ligase (PC00142) **7.04% (30)**
lyase (PC00144) **1.17% (5)**
membrane traffic protein (PC00150) **3.05% (13)**
nucleic acid binding (PC00171) **7.04% (30)**
oxidoreductase (PC00176) **4.46% (19)**
phosphatase (PC00181) **2.82% (12)**
protease (PC00190) **2.11% (9)**
receptor (PC00197) **1.64% (7)**
signaling molecule (PC00207) **3.76% (16)**
structural protein (PC00211) **0.47% (2)**
transcription factor (PC00218) **1.41% (6)**
transfer/carrier protein (PC00219) **2.11% (9)**
transferase (PC00220) **9.15% (39)**
transmembrane receptor regulatory/adaptor protein (PC00226) **0.70% (3)**
transporter (PC00227) **2.58% (11)**

Total=426

B

12.7% of total SNO-Ps shared

nuclear SNO-P dataset

cytoplasmic SNO-P dataset

122

492   348

C

SNO-proteins
nuclear extracts

3.23% (4) chromosome
13.71% (17) cytoplasm
0.81% (1) cytoskeleton
2.42% (3) cytosol
1.61% (2) golgi
15.32% (19) membrane
3.23% (4) mitochondrion
54.03% (67) nucleus
0.81% (1) organelle lumen
2.42% (3) ribosome
2.42% (3) spliceosomal complex

Total=124

SNO-proteins
cytoplasmic extracts

50.75% (34) cytoplasm
4.48% (3) cytoskeleton
38.81% (26) membrane
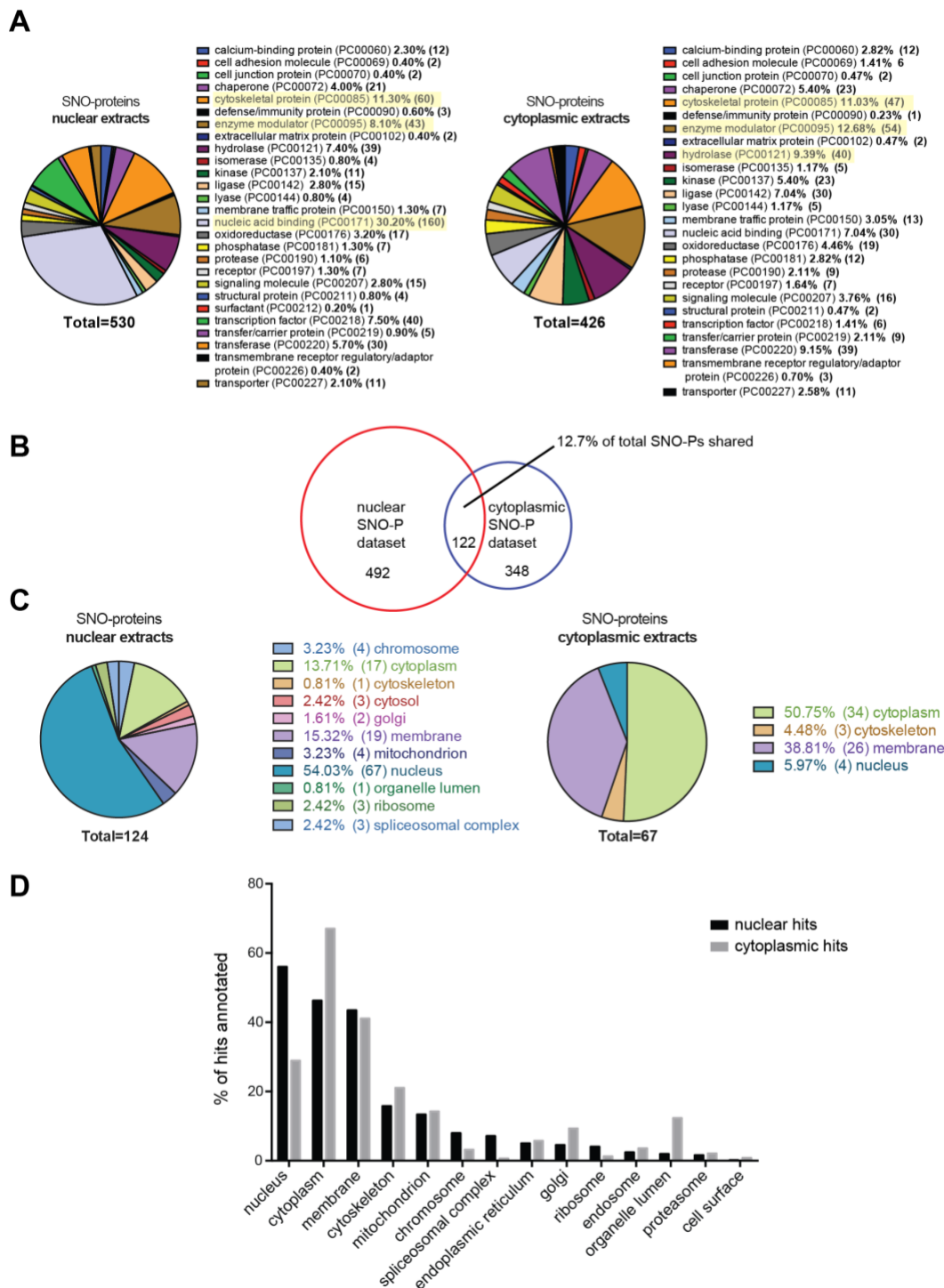5.97% (4) nucleus

Total=67

D

Fig. S3. Gene Ontology Standard Classifications. GO analysis of S-nitrosylated hits listed in **Table S2**. **(A)** Protein Class (PANTHER, version 11.1); 530 annotations were assigned for S-nitrosylated proteins identified in nuclear extracts, 426 annotations for cytoplasmic S-nitrosylated proteins. The three most commonly annotated terms for each dataset are highlighted in yellow. **(B)** Overlap between nuclear and cytoplasmic SNO-P datasets. **(C)** Exclusive annotations for cellular component

(Uniprot terms as assigned by Proteome Discover software). The number of times a particular term is assigned unambiguously, i.e. when no other term is present are shown. **(D)** Total annotations for cellular component (Uniprot terms, Proteome Discover). The percentage of annotated hits that were assigned each particular term. This includes the majority of cases in which multiple terms were assigned.
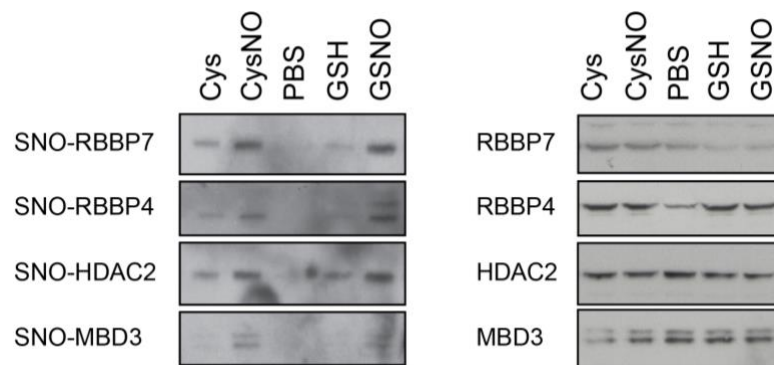
Figure S4

Fig. S4. GSNO-dependent S-nitrosylation of HDAC2, RBBP7, RBBP4 and MBD3. Neurons were treated with Cys, CysNO, GSH or GSNO (200 μM for 20 mins) and S-nitrosylated proteins isolated by biotin switch (representative blots, n=2 independent experiments). Western blot was carried out on biotin switch samples and inputs using the displayed antibodies.

Figure S5
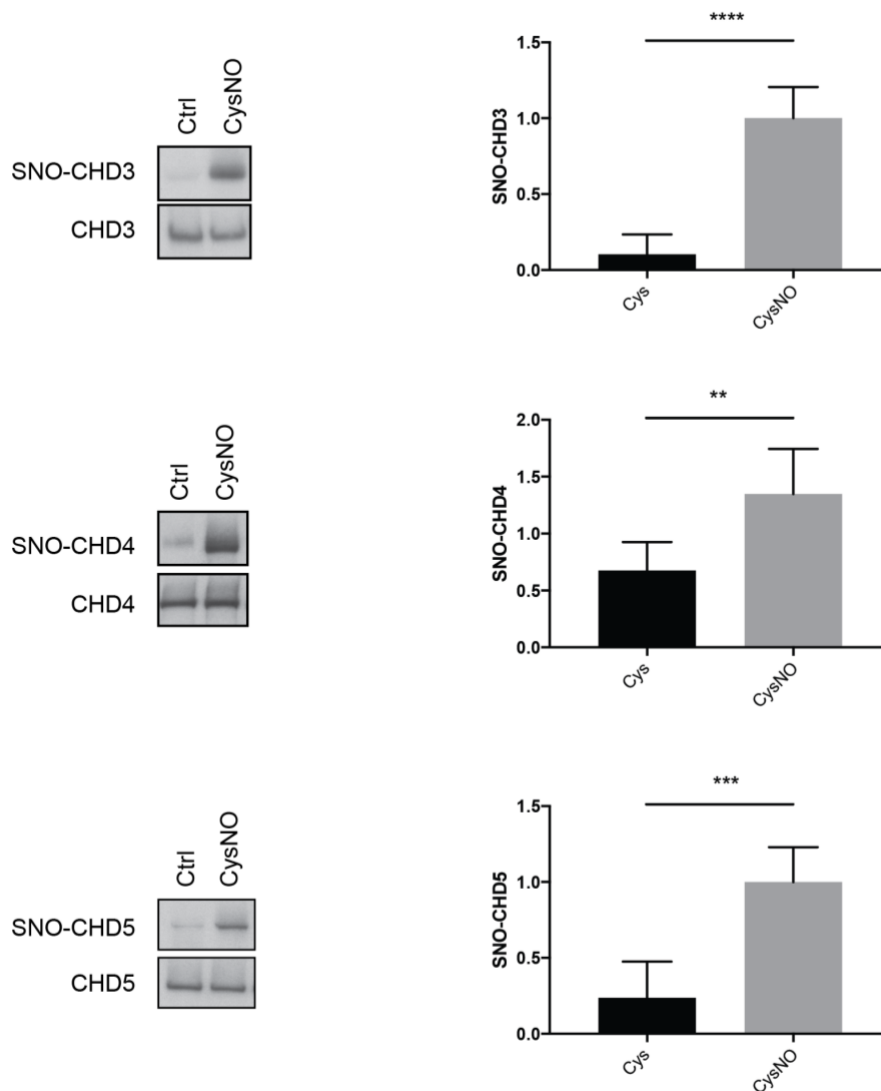
Fig. S5. S-nitrosylation of CHD3, CHD4 and CHD5. Vectors expressing flag-tagged hCHD3, mCHD4 and hCHD4 were transfected in HEK293T cells. After 48h, cell lysates were treated with Cys or CysNO (200µM for 20 mins) and subjected to the biotin switch assay using NEM (n=3 independent experiments) or MMTS (n=3 independent experiments) blocking conditions. Data was combined for densitometry analysis. Isolated proteins and total inputs were separated by SDS-PAGE followed by immunoblotting using a flag antibody. Densitometry analysis was carried out using ImageJ. SNO-signals were normalised to total inputs and expressed as fold change relative to CysNO. All data are shown as mean +/- SEM (n= 6), **p<0.01, ***p<0.001, ****p<0.0001 unpaired t-test.
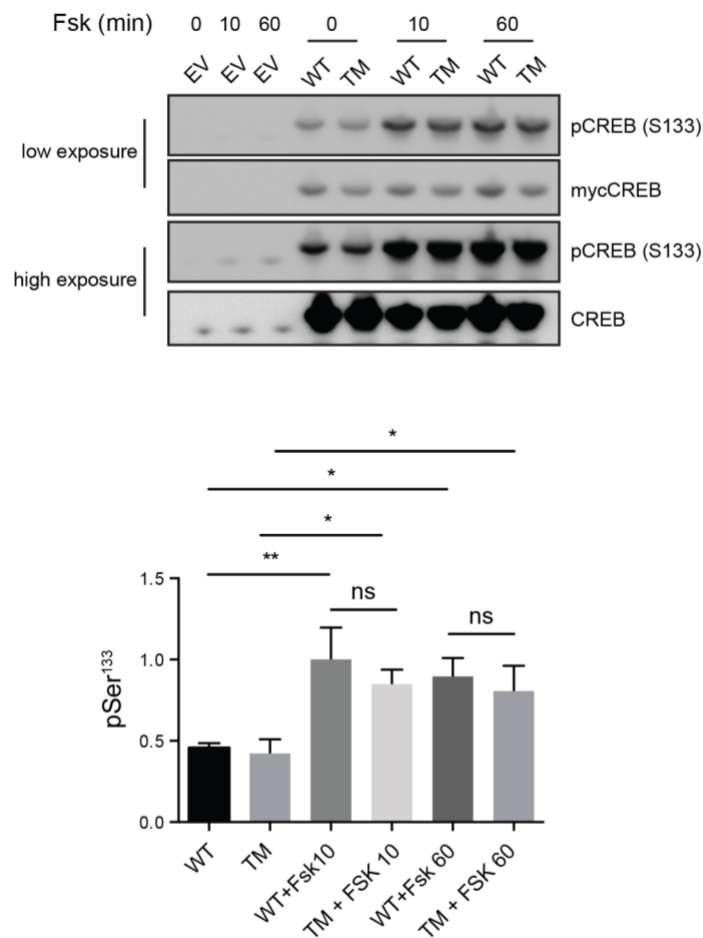
Figure S6

Fig. S6. CREB phosphorylation at serine 133 is unaffected in C300/310/337S mutant. HEK293T cells were transfected with empty vector (EV), myc-tagged wildtype (WT) or C300/310/337S mutant (triple mutant; TM) CREB and after 48h, were treated with forskolin (50µM for 10 or 60 minutes). Proteins from cell lysates were separated by SDS-PAGE followed by western blotting using an antibody against CREB phosphoserine 133 (pS133). Expression levels of transfected plasmids were assessed with myc antibody and endogenous CREB levels were assessed using a CREB antibody. Densitometry analysis on western blots was carried out using ImageJ; pS133 signals were normalised to mycCREB, and values expressed as fold change of the pS133 signal in WT mycCREB upon 10 mins FSK treatment. All data are shown as mean +/- SEM. One way ANOVA, Fisher's LSD, $*p<0.05$, $**p<0.01$, ns= not significant, n=3 independent experiments.
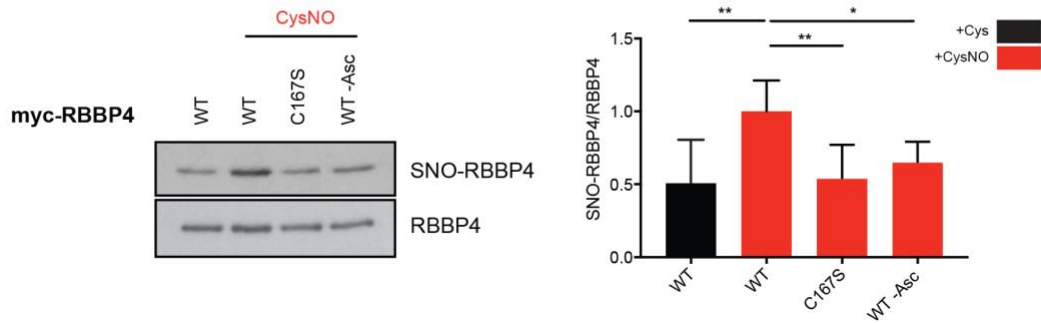
Figure S7

A
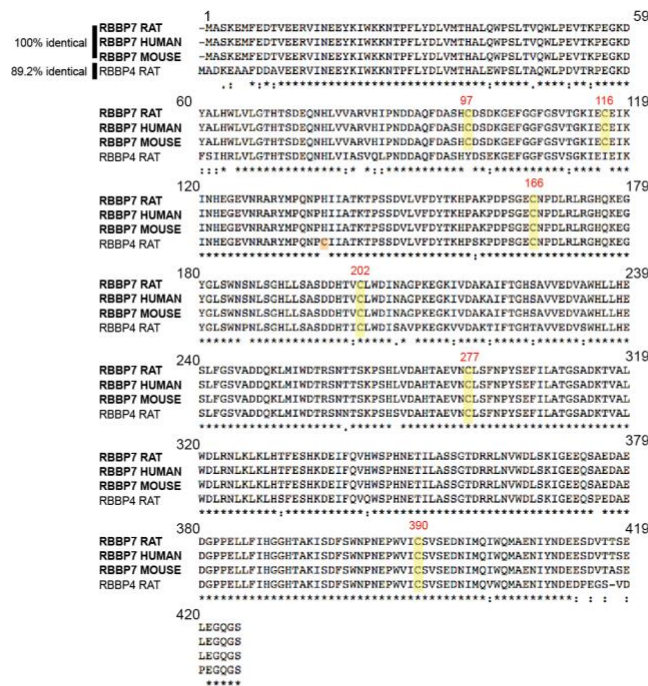
B

Fig. S7. RBBP7/4 sequence conservation and SNO-site analysis for RBBP4 and MBD3. (A) Sequence homology between rat, human and mouse RBBP7 and rat RBBP4. Sequence alignment carried out using Clustal Omega (Embl-Ebi). **(B)** Vectors expressing myc-tagged wild type rtRBBP4 (WT) or RBBP4 cysteine 167 to serine mutant (C167S) were transfected in HEK29sT2 cells. 48h after transfection cells were treated with Cys or CysNO and lysates subjected to biotin switch assay. Isolated proteins and total inputs were separated by SDS-PAGE followed by immunoblotting using a myc antibody. Densitometry analysis was carried out using ImageJ. SNO-signals were first normalised to total inputs and expressed as fold change relative to WT +CysNO. All data are shown as mean +/- SEM. *$p<0.05$, **$p<0.01$, One-way ANOVA compared to WT +CysNO column, Fisher's LSD. (B) n=6 independent experiments.
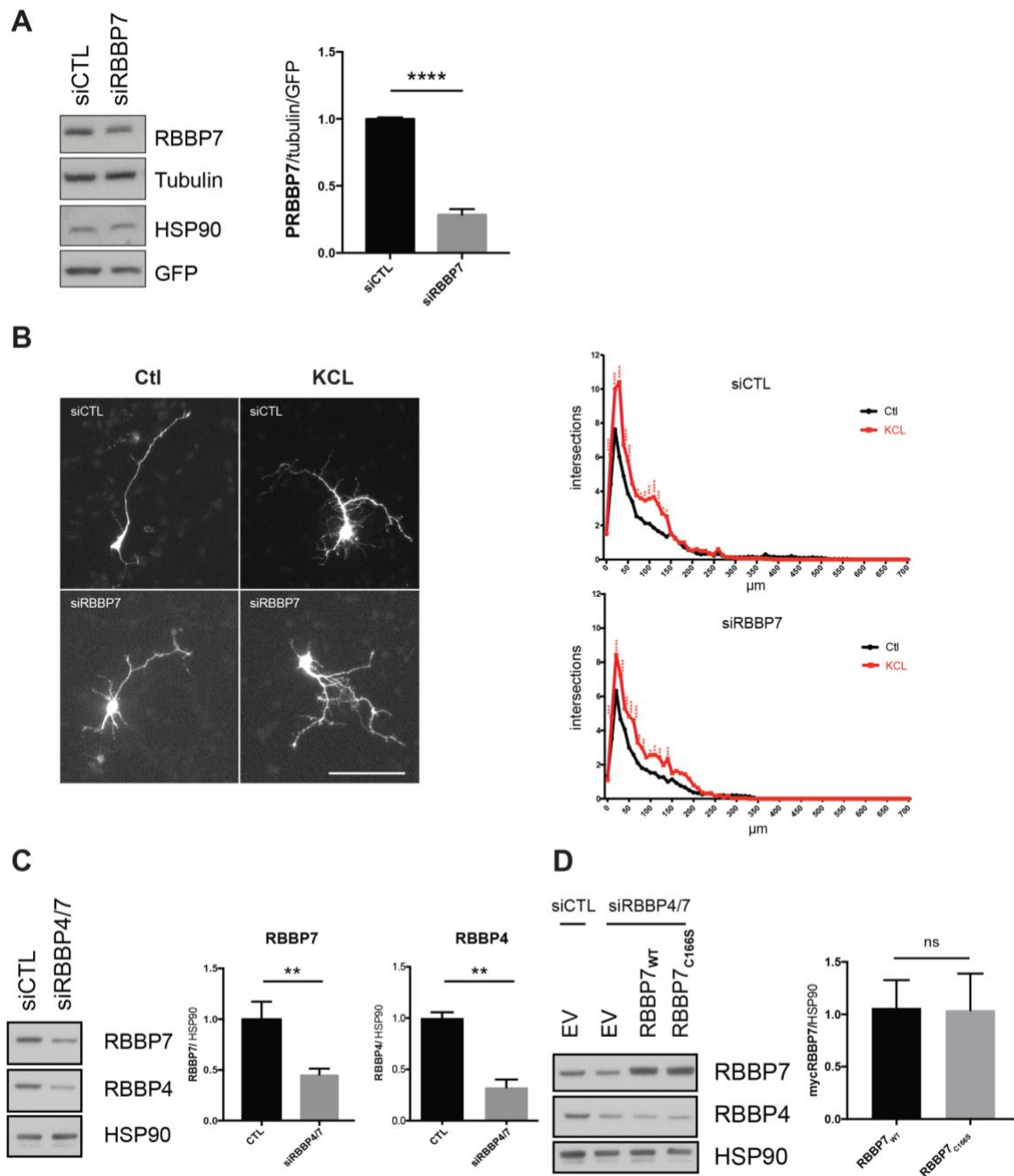
Figure S8

Fig. S8. RBBP7 knockdown and dentritogenesis analysis. **(A).** RBBP7 knockdown in N2a cells. N2a cells were transfected with a GFP expression vector together with 200nM of either control siRNA (CTL) or targeting RBBP7 (siRBBP7). Cells were harvested 48h after transfection. Western blot analysis of RBBP7, tubulin, HSP90 and GFP levels. Densitometry analysis of western blots was carried out using ImageJ. RBBP7 signal normalised to tubulin and GFP. **p<0.01 unpaired t-test. n=3 independent experiments. **(B)** RBBP7 knockdown on activity-induced dentritogenesis in cortical

neurons. Control siRNA (CTL) or siRNA against RBBP7 (siRBBP7) was transfected into E15 mouse cortical neurons alongside a GFP expression vector and mycEV. Neurons were maintained in normal media (Ctl) or in the presence of 50mM KCl (KCl) for 2 days then immunostained using an anti-GFP antibody. Images were analysed using Fiji Sholl plugin. Maximal projections show representative neurons for each condition. Scale bar 100μM. Summary of Sholl data for each condition is shown. 3 biological replicates were carried out and 10 neurons analysed per experiment (30 neurons in total). Shown are the mean values for number of intersections (y axis) against distance from soma (x axis; μm). Readings were taken every 10μm. *$p < 0.05$, **$p < 0.01$, ***$p < 0.001$, ****$p < 0.0001$ two-way ANOVA with Sidak's test for multiple comparisons. Red stars indicate KCl value is significantly greater than Ctl. **(C)** Confirmation of RBBP4/7 double knockdown. 2a cells were co-transfected with GFP expression vector and 400nM total RNA of either control siRNA (CTL) or siRNA's against RBBP4 and RBBP7 in a 1:1 ratio (siRBBP4/7). Cells were harvested 48hrs post transfection and analysed by Western blot. Western blot of RBBP7, RBBP4 and HSP90 is shown. Densitometry analysis of western blots carried out using ImageJ. RBBP7 and RBBP4 levels were normalised to HSP90. All data are shown as mean +/- SEM. **$p < 0.01$, unpaired t-test (n=3 independent experiments). **(D)** Expression of siRNA-resistant myc-RBBP7$_{WT}$ RBBP7$_{C166S}$. N2a cells were transfected with either myc-EV, siRNA-resistant myc-RBBP7$_{WT}$ or RBBP7$_{C166S}$ and siRNA CTL or the double knockdown siRBBP4/7. 48hrs after transfection cells were harvested and levels of RBBP7, RBBP4, HSP90 analysed by Western blot. RBBP7 levels in RBBP7$_{WT}$ and RBBP7$_{C166S}$ conditions were quantified by densitometry, using HSP90 as a loading control. ns= not significant (unpaired t-test, n=3 independent experiments). Data are shown as mean +/- SEM.

Supplemental Materials:

Tables S1-S15: included as separate datasets.

Legends for Tables S1-S15: included as a separate file.